NASA TECHNICAL MEMORANDUM

NASA TM X-944

50p.

FLIGHT INVESTIGATION OF A SOLAR ORIENTATION CONTROL SYSTEM FOR SPACECRAFT

by Anthony Fontana, Julian D. Maynard,
Marcus L. Brumfield, and Otis J. Parker
Langley Research Center
Langley Station, Hampton, Va.

NATIONAL AERONAUTICS AND SPACE ADMINISTRATION • WASHINGTON, D. C. • JANUARY 1964

FLIGHT INVESTIGATION OF A SOLAR ORIENTATION CONTROL SYSTEM FOR SPACECRAFT

By Anthony Fontana, Julian D. Maynard,
Marcus L. Brumfield, and Otis J. Parker

Langley Research Center
Langley Station, Hampton, Va.

NATIONAL AERONAUTICS AND SPACE ADMINISTRATION

For sale by the Office of Technical Services, Department of Commerce,
Washington, D.C. 20230 -- Price $1.25

FLIGHT INVESTIGATION OF A SOLAR ORIENTATION CONTROL SYSTEM FOR SPACECRAFT

By Anthony Fontana, Julian D. Maynard,
Marcus L. Brumfield, and Otis J. Parker
Langley Research Center

SUMMARY

12712

A three-axis solar orientation control system for spacecraft has been designed and built and has been tested both on the ground and in space flight to determine its capabilities. The system is simple; it is relatively compact; it has no moving parts other than a relay, solenoid valves, and a single rate gyro; and it is rugged enough to withstand severe environments, both during launch and in space. Silicon solar cells are used in the sensing elements for the pitch- and yaw-control axes, and the controlling torques for pitch, yaw, and roll are generated by simple cold gas, on-off, reaction jets.

In general, the flight test results confirmed the predicted capability of the system to efficiently orient any specified axis of a spacecraft toward the center of the solar disk with a limit cycle amplitude of no more than ±3 minutes of arc.

AUTHOR

INTRODUCTION

With the evolution of spacecraft, both manned and unmanned, it became apparent that there is a need for orientation of these spacecraft with respect to celestial bodies that have major influence upon the spacecraft, either with respect to its design, the fulfillment of its mission, or both. If consideration is given to the location of a spacecraft anywhere within the solar system, one of the most desirable directions of orientation for it as a whole, or for some of its parts, is toward the sun. This fact is brought out by consideration of possible requirements for thermal balance of the spacecraft, collection and utilization of the radiated energy of the sun, interplanetary navigation reference point, investigation of solar properties, and reference for astronomical telescopic observations.

Some of the basic design concepts of a solar orientation control system are described in reference 1, wherein a simple single-degree-of-freedom system was investigated. From these basic design concepts, a complete system was constructed and refined to more accurately control pitch, yaw, and roll and was installed on the fourth stage of a launch vehicle for flight testing. This

flight test was performed under a program for investigation of Spacecraft Orientation Control Systems and will be referred to herein as the SOCS Project. The purpose of this paper is to describe the complete solar orientation control system and to present briefly the results of investigations of its capabilities, both in the laboratory and in space flight. Only the primary results are presented without details, so as to permit dissemination of this information at the earliest possible date.

DESCRIPTION OF SYSTEM

The Project SOCS solar orientation control system is composed of three integrated and mutually complementary control systems. These three systems are namely, the pitch-axis attitude control system, the yaw-axis attitude control system, and the roll-axis rate control system. The pitch- and yaw-attitude control systems are identical, and together they are responsible for capturing the solar target from any initial orientation, orienting the roll axis of the payload toward the center of the solar disk, and maintaining the latter orientation during solar tracking. The roll-rate control system is responsible for reducing any residual spin rate of the payload about its roll axis to a level which eliminates significant cross-coupling between the roll axis and the other two axes of control. The controlling torques are normally generated by a high-thrust cold gas, on-off, reaction jet, pneumatic system. The three-axis control system is augmented, however, by a low-thrust system. This low-thrust system is activated at the end of the capture maneuver and has as its primary function the conservation of fuel. A photograph of the Project SOCS spacecraft is shown in figure 1(a) and a drawing of the spacecraft which shows the location of the major components and instrument packages is presented in figure 1(b). Weights, volumes, and electrical power consumption of the various control-system components, as installed in the SOCS Project spacecraft, are listed in table I.

Pitch- and Yaw-Attitude Control System

The pitch- and yaw-attitude control system is composed of three basic functional units: the solar sensor, the electronic processing circuitry, and the pneumatic controls. The solar sensor, by means of an electrical output signal, supplies the processing circuitry with adequate information to enable the circuitry to determine the instantaneous magnitude and direction of the angular pointing error of the roll axis of the payload relative to the solar vector. The electronic processing circuitry energizes the pneumatic controls which, in turn, supply the torques necessary for the correction of the angular pointing error. The pneumatic controls will be described in a later section of this paper.

A block diagram of the pitch- and yaw-attitude control system is shown in figure 2. A description of the circuitry of the various electronic components is presented in the appendix.

Solar sensor.- The solar sensor is actually a dual sensor composed of coarse sensing elements, which are used during capture from large error angles, and fine sensing elements, which are used during accurate pointing. Four coarse sensing elements are located at 90° intervals around the payload, as shown in figure 1. These coarse sensing elements, which are located in both the pitch and yaw axes, have a full spherical field-of-view and thus the capability of capturing the solar target from an initial error of 180°. A photograph of a single coarse sensing element is shown in figure 3. Four fine sensing elements are mounted in a fine sensor block, as shown in figures 4 and 5, and the complete fine sensor is mounted on the payload, as shown in figure 1. Due to the geometrical placement of the fine sensing elements within the sensor block, the sensing elements are shielded from the solar radiation that is reflected from the earth and are thus capable of accurate pointing toward the center of the solar disk.

Each of the coarse and fine sensing elements is composed of three silicon solar cells connected in series and mounted under a protective glass cover. Geometrically opposed sensing elements are connected in a battery bridge circuit for the purpose of obtaining a signal output with a polarity that indicates the direction of the pointing error. The magnitude of the sensor output signal indicates the magnitude of the pointing error. The composite single-axis solar sensor output characteristic is shown in figure 6, and individual coarse and fine sensor output characteristics are shown in figures 7 and 8, respectively.

Lead networks.- The output signals from the coarse and fine sensors feed into the coarse and fine lead networks, respectively. (See fig. 2.) The lead networks are simple resistance, capacitance compensation circuits which establish favorable damping coefficients for the system. The use of two lead networks makes it possible to establish an optimum damping coefficient for both the coarse and fine capture maneuvers.

Sensor switch.- The sensor switch connects the output of either the coarse lead networks or the fine lead networks to the input of the appropriate amplifiers (see fig. 2), depending upon whether the sensor switch triggering element (figs. 4 and 5) is illuminated by solar radiation. The triggering element is a photo-duo-diode, which is mounted geometrically within the fine sensor block so that it is illuminated only when both axes of the pitch- and yaw-attitude control system have a pointing error less than 22°. When the pointing error of either, or both, control-system axes is greater than 22°, the output of the coarse lead networks of both axes are connected to the appropriate amplifiers. When the pointing error of both control-system axes is less than 22°, the coarse lead networks are disconnected from the amplifiers and the fine lead networks are connected to them.

Amplifiers and valve drivers.- The solar sensor outputs pass through the lead networks and the sensor switch into the amplifiers. (See fig. 2.) The amplifiers are of the balanced d-c type and are designed to minimize d-c drift. The valve drivers actuate the proper solenoid valves, depending upon the polarity of the amplifier outputs.

Roll-Rate Control System

The roll-rate control system is composed of three basic functional units: a roll-rate sensing device, electronic processing circuitry, and pneumatic controls. The roll-rate sensing device is a gyroscope with an electrical output that enables the electronic processing circuitry to determine the magnitude and direction of the roll rate. The processing circuitry energizes the pneumatic controls which, in turn, supply the corrective torques required to reduce the roll rate. The roll-rate control system reduces the roll rate to ±0.25 rpm.

A block diagram of the roll-rate control system is shown in figure 9. The 10°-per-second rate gyroscope, with its built-in inverter and demodulator, generates the output characteristic shown in figure 10. The amplifier is basically a single stage of the balanced d-c amplifiers used in the pitch- and yaw-attitude control system. The valve driver is identical to the ones used in the pitch- and yaw-attitude control system.

Pneumatic System

The pneumatic system supplies the torques necessary for the correction of the pitch- and yaw-attitude errors and the reduction of the roll rate. The pneumatic controls are of the cold gas, on-off, reaction jet type. The fuel is nitrogen, and the reaction jets are activated by solenoid valves.

A schematic diagram of the pneumatic system is shown in figure 11. The gaseous nitrogen is stored at an initial pressure of 3,000 psi. This storage-tank pressure is reduced for use by the reaction jets by two pressure regulators. When the normally open solenoid valve is not energized, the inlet pressure to the pitch, yaw, and roll reaction jet nozzles is 40 psia, and all jets will produce a high thrust when activated. When the normally open solenoid valve is energized, the inlet pressure to the pitch and yaw reaction jet nozzles is reduced to 4 psia, and these jets will produce a low thrust when activated. More information is given on this subject in the description of the low-thrust system. The attitude jets are located in the plane of their respective coarse sensors, as shown in figure 1(b). The location of the roll jets is also shown in figure 1. These roll jets are activated in pairs, which are mounted on opposite sides of the spacecraft, to form a couple and to prevent the introduction of errors into the pitch and yaw axes. The spacecraft inertias and the thrusts of the control jets are presented in table II. Photographs of the various components of the pneumatic system are shown in figure 12. A specially designed 25-micron filter, which is shown in figure 12(d), was installed in the inlet side of all control valves.

Low-Thrust System

The three-axis control system described thus far is augmented by a low-thrust system. The low-thrust system is incorporated with the general control system for the primary purpose of conserving fuel and for the secondary purpose of reducing the amplitude of the lock-on limit cycle. At the instant when the

absolute value of the vector sum of the pointing error in both the pitch axis and the yaw axis becomes less than 1°, the low-thrust system automatically generates its own triggering signal. The triggering signal initiates a brief time delay at the end of which low-thrust operation of the pitch- and yaw-attitude control system is established. Laboratory tests indicated that the time delay is necessary to prevent the possibility of oscillating between high and low thrust.

The low-thrust system is composed of the low-thrust triggering element, the low-thrust switch, and a normally open solenoid valve. The low-thrust triggering element triggers the low-thrust switch which, after the prescribed time delay of 7 seconds, closes the normally open solenoid valve. (See fig. 11.) The closure of the normally open valve blocks the high-pressure flow of nitrogen gas to the pitch- and yaw-control jets, leaving the jets to operate from the nitrogen output of the low-pressure regulator, as explained in the previous description of the pneumatic system. While operating from a lower pressure source, the control jets will develop less thrust at a smaller flow rate of nitrogen.

Triggering method.- The low-thrust triggering element is a photo-duo-diode mounted in the fine sensor block, as shown in figure 13. (See also fig. 5.) Three 0.040-inch-diameter stops were inserted into a 1/8-inch-diameter drilled hole, and the triggering element was mounted directly behind the third stop. The diameter of the stops and the length of the hole are such that the triggering element is illuminated by direct solar radiation only when the absolute value of the resultant pitch- and yaw-axes pointing error is less than 1°. When the photo-duo-diode is illuminated, its internal resistance drops from a high value to a low value. It is this change in resistance which triggers the low-thrust switch.

Low-thrust switch.- The duty of the low-thrust switch is to activate the normally open solenoid valve (i.e., to initiate the low-pressure, low-thrust pitch and yaw control) approximately 7 seconds after the triggering element is illuminated. The switch is designed to reset instantaneously (i.e., switch back to high-pressure, high-thrust pitch and yaw control) should the resultant pitch- and yaw-axes pointing error become greater than 1°. Another design feature of the switch insures that the time delay of 7 seconds will remain constant, regardless of fluctuations or slow decays of the supply voltage.

TESTS AND RESULTS

For the purpose of carrying out both the ground testing program and the flight testing program, the spacecraft was assembled around an Altair (X-248) rocket motor, as shown in figure 1. A dummy Altair motor case was used throughout the ground testing program.

Ground Tests

The ground testing program was designed to attain three primary objectives. The first objective was to obtain a preliminary confirmation of the design theories and concepts through extensive functional and performance testing of the complete three-axis control system. The second objective was to compile a sufficient amount of performance data to accurately specify the capabilities of the three-axis control system. The third objective was to obtain a confirmation that the payload could withstand the environmental conditions to which it would be exposed during its flight test.

Pitch- and yaw-attitude control-system tests.- The performance testing of the pitch- and yaw-attitude control system consisted of four basic tests. These four tests were, namely: the capture tests, the initial pitch- and yaw-rate tests, the limit cycle tests, and the fuel-consumption tests. Figure 14 is a photograph of the test setup. The spacecraft was mounted on an air bearing to allow relatively friction-free angular movements. A mercury xenon solar simulator provided the necessary radiation for the series of tests. Only a single axis of the attitude control system was placed under test at any one time; therefore, the data to be presented are single-axis data unless otherwise specified. All angular measurements were made by an optical system throughout the series of tests.

The capture tests of the pitch- and yaw-attitude control system were performed to confirm the capability of the system to capture the solar target, regardless of its initial orientation. The single-axis performance data obtained from the capture tests are presented in figure 15. The control system was considered to have captured the solar target when the pointing error of the axis being tested had been reduced to 1°. One minute of time was required to lock on to the center of the solar disk (i.e., attain limit cycle operation) from a pointing error of 1° of arc.

The initial angular rate tests were performed to determine the capability of the pitch- and yaw-attitude control system to stop angular movements. The tests were conducted with the initial rate applied both in a direction such as to decrease the pointing error of the axis under test and in such a direction as to increase the pointing error of the axis under test. The latter direction of application of the initial angular rates proved to be the critical one with respect to preventing the spacecraft from tumbling, and the data obtained from these tests are presented in figure 16. If the data given in table II are used to calculate the time required to overcome various initial angular rates and to calculate the angular movement traversed in overcoming these initial angular rates, it will be discovered that there is some disagreement between the calculated data and the actual ground test data presented in figure 16. The primary reason for the disagreement is the change in inertia of the spacecraft that occurred during the few weeks after the completion of the ground testing program and prior to the final measurement of the spacecraft inertias.

The limit cycle tests of the pitch- and yaw-attitude control system were performed for the primary purpose of determining the amplitude of the

oscillation about zero pointing error. The attainment of a limit cycle indicates that the attitude control system has locked on to the center of the solar disk with its best obtainable accuracy. The test results revealed the limit cycle amplitude to be ±3 minutes of arc if operating on high thrust and ±1 minute of arc if operating on low thrust.

The fuel consumption tests of the pitch- and yaw-attitude control system were performed to confirm the calculated rate of fuel usage. The fuel-consumption rate of the two-axis attitude control system while capturing (two jets on constantly) the solar target is 0.130 pound of nitrogen per minute of time. The fuel-consumption rate of both axes during limit cycle operation and while on high thrust is 0.104 pound of nitrogen per minute of time. While on low thrust and during limit cycle operation, the fuel consumption rate in both axes is 0.010 pound of nitrogen per minute of time.

Roll-rate control-system tests.- The performance testing of the roll-rate control system was performed in the simulated space environment created by a vacuum sphere and an air bearing support system. Figure 17 is a photograph of the test setup. The roll-rate tests were performed to confirm the capability of the roll-rate control system to reduce any residual spin rate of the spacecraft about the roll axis to ±0.25 rpm. The results of the roll-rate test are presented in figure 18. If the data given in table II are used to calculate the time required to reduce various initial roll rates to ±0.25 rpm, it will again be discovered that there is some disagreement between the calculated data and the actual ground test data presented in figure 18. Changes in the inertia of the spacecraft between the completion of the ground testing program and the measurement of the final spacecraft inertias account for a major part of the disagreement. The fuel-consumption tests of the roll-rate control system revealed the rate of fuel usage to be 0.166 pound of nitrogen per minute while in the process of reducing the roll rate to ±0.25 rpm. Results of the laboratory tests confirmed that the dead band of ±0.25 rpm allows a considerable reduction in fuel consumption and that a roll rate of ±0.25 rpm is sufficiently small to eliminate all significant cross coupling between the control axes.

Environmental tests.- The Project SOCS environmental test program was designed to prove the spacecraft capable of withstanding both the environment created by the launch vehicle and the space environment. The spacecraft was subjected to the appropriate environmental tests, both as an assembled package and as individual components. The environmental test magnitudes for those tests simulating the environment created by the launch vehicle were based on the available data describing the past performance of the particular launch vehicle and do not necessarily represent the maximum magnitudes which the spacecraft and its components can withstand. However, the rough burning of the solid-fuel rocket motors of the launch vehicle and the spin stabilization of the fourth stage represent sufficiently rigorous environmental conditions to insure that the system is capable of withstanding severe launch environments.

The environmental test magnitudes for the individual spacecraft components are presented in table III. Due to the spin stabilization of the spacecraft stage of the launch vehicle, the critical transverse accelerations are created by centrifugal forces and thus depend upon the radial mounting location of the

individual component. The transverse acceleration test magnitudes for the major spacecraft components are presented in table III(b). The thermal test magnitudes also depend upon the physical location of the individual component and are thus presented in table III(b).

The completely assembled spacecraft was subjected to a shock test at the magnitude specified for the shock test of individual components in table III. For the purpose of making the vibration tests, the spacecraft was divided into two subassemblies, one consisting of that portion of the spacecraft located forward of the Altair rocket motor and the other consisting of that portion of the spacecraft located around the nozzle of the Altair rocket motor. Although the two subassemblies were tested separately, the two were electrically connected during the tests. The general vibration tests of the subassemblies were made at 50 percent of the magnitudes specified for the general vibration test of the individual components in table III, while the special vibration tests of the subassemblies were made at the magnitudes specified for the special vibration test of the individual components in table III. The completely assembled spacecraft was spun at 400 rpm about its roll axis to provide a realistic transverse acceleration test. Thermal, vacuum, and longitudinal acceleration tests were not performed on the assembled spacecraft.

Flight Test

The flight test of the Project SOCS spacecraft was performed to provide flight confirmation of the design concepts of the spacecraft in a space environment. The flight test was conducted from the NASA Wallops Station launch range on September 20, 1963, at 10:46 a.m., e.s.t. The performance of the three-axis control system was monitored by an 18-channel FM/FM telemeter. Figure 19 is a photograph of the four-stage vehicle and the spacecraft on the launcher.

The Project SOCS experiment began at an altitude of 409,000 feet when the solar sensors were exposed to solar radiation by the ejection of the heat shield. The apogee of the flight trajectory was 1,054,252 feet. The experiment was terminated at an altitude of approximately 470,000 feet and had a duration of 7.1 minutes. Six channels of continuous telemeter data, which describe the pitch and yaw performance of the spacecraft during the entire period of the experiment, are presented in figures 20 and 21. Figure 20 presents the pitch-axis data which were obtained from the pitch-axis solar sensors and figure 21 presents the yaw-axis data which were obtained from the yaw-axis solar sensors. In both figure 20 and figure 21 the coarse solar sensors provided the control information for the spacecraft until the actuation of the sensor switch at 68 seconds of experiment time. After actuation of the sensor switch, the control information for the spacecraft was supplied by the fine solar sensor. The channel-number-1 fine sensor data and the channel-number-2 fine sensor data were obtained from the same source but were completely isolated thereafter, since they had no common components in the telemeter. Channel number 1 allows the fine sensor output to be monitored at pointing errors as great as 25° with an accuracy of $\pm 1.25^{\circ}$. Channel number 2 allows the fine sensor output to be monitored at pointing errors less than 1° with an accuracy

of ±3 minutes of arc. Although the output of the fine sensor was monitored continuously and all the data obtained during the experiment are presented in figures 20 and 21, the channel-number-1 and channel-number-2 fine sensor data are ambiguous until after the actuation of the sensor switch, because of the geometric characteristics of the fine sensor.

At the beginning of the experiment, the pitch-axis pointing error was 2.7° and the yaw-axis pointing error was 11.4°, as shown by the coarse sensor data of figures 20 and 21, respectively. The initial angular rates in both the pitch and yaw axes were in a direction such as to increase the pointing error of those axes. (See figs. 20 and 21.) Concurrence between the data obtained from the coarse sensors and the data obtained from the fine sensor at the time of sensor-switch operation was not expected since the output of the coarse sensors is influenced by solar radiation that is reflected from the earth. Actuation of the sensor switch occurs when the absolute value of the vector sum of the pitch-axis pointing error and the yaw-axis pointing error becomes approximately 22°. At the instant of actuation of the sensor switch, the pitch-axis fine sensor (channel number 2) indicated an error of 0.7° and the yaw-axis fine sensor (channel number 1) indicated an error of 3.5°, revealing a discrepancy in the data, since the absolute value of the vector sum of these two errors is only 3.6°. A detailed analysis of the 18 channels of telemetered data covering such items as angular velocities, reaction jet operation, fuel consumption, etc., supports the belief that all the pitch-axis data and yaw-axis data that were obtained from the coarse sensors are entirely trustworthy. The detailed analysis of the available telemetered data, analysis of ground test data, and consideration of the fine sensor geometry reveal beyond reasonable doubt that the data obtained from the yaw-axis fine sensor (channel number 1) between 52 and 75 seconds of experiment time are not trustworthy since these data describe a situation which is physically impossible in that, with a relatively small pointing error in the pitch axis, it is impossible to capture from an error angle greater than 22° to a small error in the yaw axis without receiving an indication from the yaw-axis fine sensor (channel number 1) of a pointing error of approximately 25°, which is the full-scale output of the fine sensor. (See fig. 8.) The dashed portion of the yaw-axis fine sensor data (channel number 1, fig. 21) was obtained through extrapolation of the data that are considered trustworthy, using ground test data as a general guide. The extrapolated data of figure 21 describe the performance of the yaw axis of the attitude control system between 52 and 75 seconds of experiment time in a physically realizable manner. The channel-number-1 yaw-axis fine sensor data are considered to be trustworthy from 75 seconds of experiment time to the end of the experiment because of their close correlation with the channel-number-2 data of the same axis.

Figure 22 presents a cross plot of the data presented in figures 20 and 21 and gives an indication of the ability of the two-axis attitude control system to logically perform its mission in the presence of the cross coupling introduced by the continuous motion of the spacecraft about its roll axis. The coarse-sensor data are plotted from the beginning of the experiment to point A of figure 22, where the sensor switch was actuated and control of the spacecraft was shifted to the fine sensors. Point B is the indicated pointing error of the fine sensors at the instant of actuation of the sensor switch. A portion

of the curve presented in figure 22 is dashed to represent the extrapolated data of figure 21 that were used in making the cross plot. The discontinuity of the cross plot between points A and B is produced by the erroneous indication of the coarse sensors, whose output signal is contaminated by earth-reflected solar radiation.

The data obtained from the telemetry channels that monitored the pitch and yaw nozzle inlet pressures, the pitch and yaw angular velocities, the pitch and yaw fuel-consumption rate, and the voltage across the normally open solenoid valve coil, indicate conclusively that the low-thrust system failed to operate, even though there was a period of more than 1 minute of experiment time during which the absolute value of the resultant pitch and yaw pointing error was less than 1°. The telemetry data give no hint as to the nature of the failure of the low-thrust system; the failure could have been in the optics of the low-thrust triggering scheme or in the electronics of the low-thrust switch.

The limit cycle amplitude in the pitch axis was ±3 minutes of arc about a pointing error of 1° of arc. (See fig. 20.) The limit cycle amplitude in the yaw axis was ±3 minutes of arc about a pointing error of 15 minutes of arc. (See fig. 21.) The apparent failure of the pitch- and yaw-attitude control system to attain a limit cycle that oscillated about zero pointing error is assumed to have been caused by stray, off-setting biases which were generated somewhere within the electronics of the control system or telemetry. The off-setting biases could have been in the form of d-c drift in the control-system amplifiers or in the form of zero shifts in the telemetry. Both preflight and postflight laboratory tests of the control-system amplifiers indicate that it is highly improbable that the d-c drift of the amplifiers could have accounted for more than 1 minute of arc of pointing error.

The fuel-consumption rate of the pitch- and yaw-attitude control system was 0.134 pound of nitrogen per minute of time during limit cycle operation. The fuel-consumption rate during the capture maneuver is not available, since the nitrogen storage tank was charged to 3,200 psi before the flight test, causing the monitoring pressure transducer to indicate its maximum reading of 3,000 psi throughout the duration of the capture maneuver.

The residual roll rate of the spacecraft about its roll axis, at the beginning of the space flight test of the SOCS payload, was 0.16 rpm as evidenced by the frequency of the sinusoidal output of the coarse sensors of both the pitch and yaw axes. (See figs. 20 and 21.) The sinusoidal outputs of the pitch and yaw coarse sensors, which are of equal amplitude and 90° out of phase, are produced by the coarse sensors in response to earth-reflected solar radiation while rolling at a small rate. With a roll rate of only 0.16 rpm, the roll-rate control system was not called upon to function throughout the usable flight test time. The operational status of the roll-rate control system was verified, however, when the pyaload orientation was disturbed by atmospheric reentry forces.

During the launch phase of the flight test the Project SOCS spacecraft was subjected to a maximum vibration of ±20g at 50 cps, a maximum thrust-axis acceleration of 27g, and a maximum spin rate of 420 rpm. The electronic control-system components were exposed to a maximum temperature of 28° C, and the

pneumatic control-system components were exposed to maximum temperatures that varied from 48° C to 82° C, depending upon the location of the component.

CONCLUDING REMARKS

An integrated three-axis solar orientation control system for spacecraft has been designed and built and has been tested both on the ground and in space flight to determine its capabilities. The system is simple; it is relatively compact; it has no moving parts other than a relay, solenoid valves, and a single rate gyro; and it is rugged enough to withstand severe environments, both during launch and in space. Silicon solar cells are used in the sensing elements for the pitch- and yaw-control axes, and the controlling torques for pitch, yaw, and roll are generated by simple cold gas, on-off, reaction jets.

Where valid comparisons can be made between the ground and flight test results, such comparisons indicate general agreement. Therefore, it may be concluded that, in general, the flight test results confirmed the predicted capabilities of the control system. The flight test showed that the solar orientation control system was capable of effecting a capture maneuver from sizable error angles, and with initial angular rates in a direction such as to increase the pointing error in both the pitch and yaw axes. Furthermore, the flight test confirmed the value of the coarse-fine sensor design feature, which reduced the pointing error to less than 1° after only 100 seconds of experiment time. The predicted limit cycle amplitude for high-thrust operation was confirmed by the flight test. Although the residual roll rate about the roll axis was sufficiently low throughout the flight experiment time so that the roll-rate control system was not called upon to function, this small roll rate was sufficient to provide a check on the capability of the system to function properly with small cross-coupling effects between the axes of the control system. Finally, the rough burning solid-fuel rocket motors of the launch vehicle and the spin stabilization of the fourth stage represented sufficiently severe environmental conditions to confirm that the system has the capability to withstand high vibratory and acceleration forces.

Langley Research Center,
National Aeronautics and Space Administration,
Langley Station, Hampton, Va., December 26, 1963.

APPENDIX

CIRCUIT DIAGRAMS

The solar sensor schematic diagram is shown in figure 23. Resistors R_1, R_2, R_3, and R_4 load the sensors and control the slope of their output characteristics.

The resistance and capacitance values of the lead networks are given in figure 24, which is a schematic diagram of the lead networks.

Figure 25 is a schematic diagram of the sensor switch. Transistors T_1 and T_2 are connected in a circuit to take advantage of the gain of T_1 and the collector current capacity of T_2 while using only one power supply. Capacitor C_1 and diode D_1 form a transient suppression circuit which protects the transistors from the relay coil transient current. The relay is used to allow simple circuit design and to provide absolute isolation of the switching contacts to insure that the solar sensor outputs are not contaminated by electronic noise and stray bias currents. Potentiometer P_1 is used to adjust the triggering current of the switch. This potentiometer is adjusted so that solar radiation incident upon the triggering element at an angle of 22° is sufficient to trigger the switch; the reflected radiation from the earth, which is of lesser intensity, is insufficient to trigger the switch. Thus, the control system is able to discriminate between the earth and the sun to avoid the possibility of capturing the earth.

A schematic diagram of the amplifier is shown in figure 26. Transistors T_1 and T_2 are manufactured in a single hermetically sealed case, as are transistors T_3 and T_4. The common case maintains a mutual operating temperature for the two transistors and reduces d-c drift and the possibility of thermal run-away. The negative feedback resistors R_1, R_2, R_3, and R_4 and a common heat sink, within which all critical circuit components are mounted, further reduced d-c drift. Precision, low-temperature-coefficient resistors are used exclusively throughout the amplifier circuit. Potentiometers P_1 and P_4 provide a means of adjusting the gain of the amplifier, and potentiometers P_2, P_3, P_5, and P_6 provide a means of balancing the amplifier stages.

A schematic diagram of the valve driver is shown in figure 27. Diodes D_3 and D_4 make the switch sensitive to polarity. Capacitors C_1 and C_2 and diodes D_1 and D_2 form transient suppression networks which protect the transistors from the transient current produced by the collapse of the magnetic field of the solenoid valve coils during switching operations.

A schematic diagram of the roll amplifier is shown in figure 28. The major difference between the roll amplifier and the pitch and yaw amplifiers is the

use of relatively low-gain transistors, which allow a few circuit simplifications. Capacitors C_1 and C_2 filter the 400-cycle-per-second ripple from the rate-gyroscope output. This 400-cycle-per-second ripple is characteristically impressed upon the gyroscope output by its inverter.

A schematic diagram of the low-thrust switch is shown in figure 29. Capacitor C_1 and resistor R_3 establish the 7-second time delay. Resistor R_2 and zener diode Z_1 provide a constant reference voltage for the time-delay circuit, regardless of any fluctuations in the supply voltage. Zener diode Z_2 generates the pulse necessary to trigger the silicon controlled switch S_1. The pulse is generated at the end of the time delay. The resistor R_4 is a discharge resistor for the time-delay circuit. This resistor begins to reset the time-delay circuit when S_1 is triggered so that if a momentary disturbance causes the resultant pointing error to become greater than 1°, the full time delay of seven seconds will again occur when the resultant pointing error returns to less than 1°. The sensitivity of the switch is adjusted by potentiometer P_1. Capacitors C_2 and C_3 and diode D_1 protect the transistors and the silicon controlled switch from damaging transient currents.

REFERENCE

1. Salmirs, Seymour, Kessler, S. Lawrence, and Parker, Otis J.: A Simple Solar Orientation Control System for Space Vehicles. NASA TN D-1271, 1962.

TABLE I.- SPACECRAFT AND COMPONENTS; WEIGHTS, VOLUMES,

AND ELECTRICAL POWER CONSUMPTION

Component	Number of components per spacecraft	Weight per component, lb	Volume per component, $in.^3$	Electrical power consumption per component, w
Coarse solar sensor	4	0.05	0.70	-----
Fine solar sensor	1	.99	15.80	-----
Lead network	1	1.02	17.72	-----
Sensor switch	1	.39	8.37	0.84
Low-thrust switch	1	.64	12.47	.84
Amplifier and valve driver combination	3	1.09	17.72	.18
Rate gyroscope	1	.69	8.12	5.40
Nitrogen storage tank	1	10.15	470.00	-----
Nitrogen	-	3.12	------	-----
40 psia regulator	1	1.13	13.59	-----
4 psia regulator	1	1.34	18.43	-----
Normally closed solenoid valve	8	.30	1.53	14.00
Normally open solenoid valve	1	.32	1.53	14.00
Pitch or yaw nozzle	4	.03	.12	-----
Roll nozzle	4	.01	.23	-----
Electrical wiring[a]	-	5.00	150.00	
Pneumatic tubing[a]	-	5.00	45.00	

[a]Estimated.

Total weight - 35.82 lb
Total volume - 830.63 $in.^3$
Total power consumption - 133.62 w

TABLE II.- FLIGHT THRUSTS AND INERTIAS

Axis	Inertia, slug-ft^2	Thrust, lb		Jet moment arm, ft
		Low	High	
Pitch	52.3	0.0066	0.066	2.89
Yaw	52.3	.0066	.066	2.89
Roll	4.7	------	[a].086	.95

[a]Thrust of a single roll jet.

TABLE III.- ENVIRONMENTAL TEST MAGNITUDES

FOR INDIVIDUAL SPACECRAFT COMPONENTS

(a) Environmental test magnitudes independent of component location

Test	Magnitude	
	Transverse axis	Longitudinal axis
General vibration	±2g at 20 to 100 cps ±4g at 100 to 500 cps ±6g at 500 to 2,000 cps	±4g at 20 to 100 cps ±14g at 100 to 500 cps ±28g at 500 to 2,000 cps
Special vibration	±10g at 550 to 650 cps	±45g at 550 to 650 cps
Shock		30g for 10 milliseconds
Acceleration	See (b) below	50g
Vacuum	10^{-7} mm Hg	

(b) Environmental test magnitudes dependent on component location

Component	Magnitudes		
	Transverse acceleration, g	Temperature, °C	
		Minimum	Maximum
Coarse solar sensor	160	0	100
Fine solar sensor	0	0	100
Rate gyroscope	0	-	74
Sensor switch	45	-	74
Low-thrust switch	45	-	74
Lead network	90	-	---
Amplifier	90	-	49
Power switch	90	-	49
Regulators	140	-	74
N. O. solenoid valve	140	-	74
N. C. solenoid valves	160	-	74

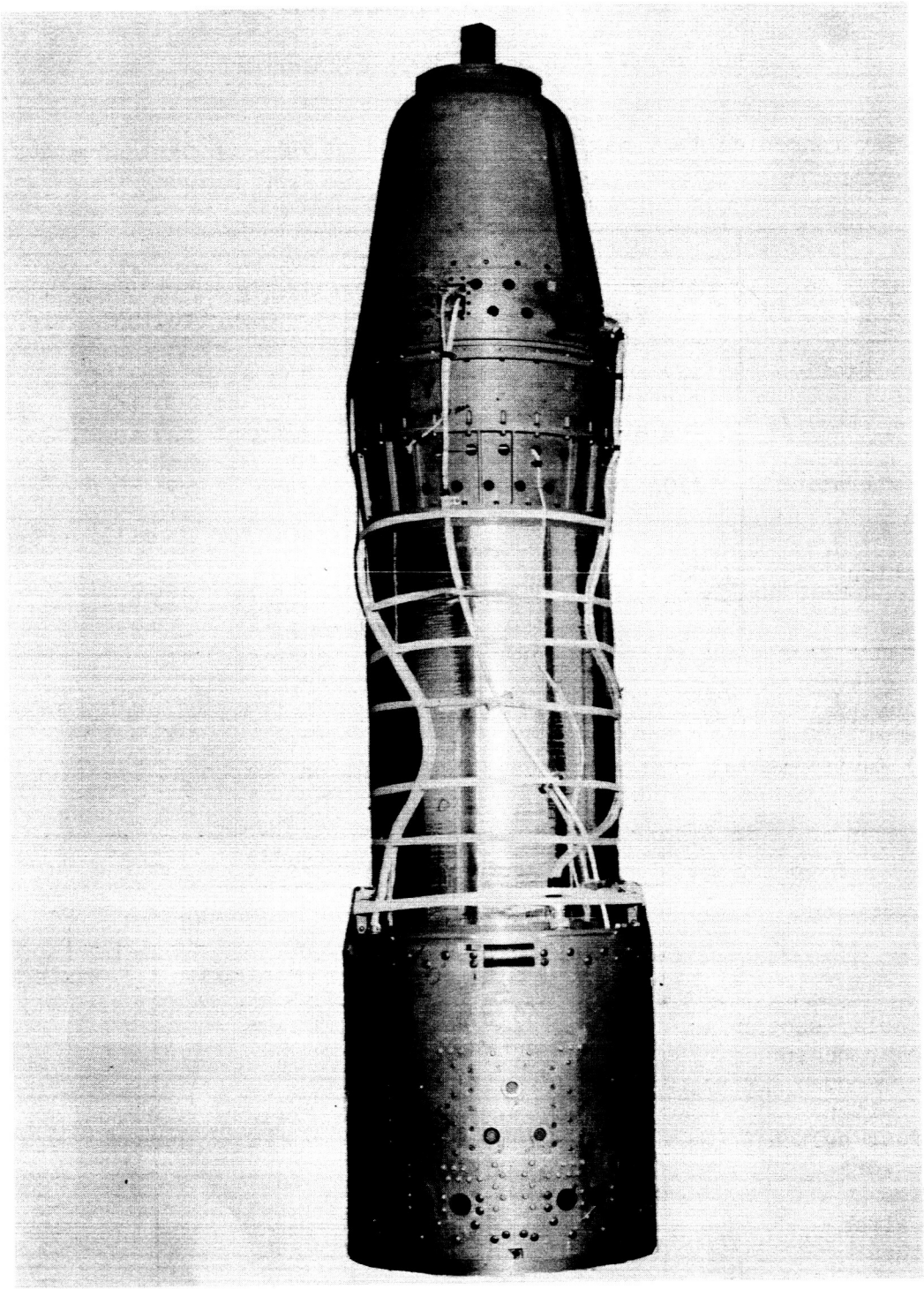

(a) Photograph. L-63-6790

Figure 1.- SOCS Project spacecraft.

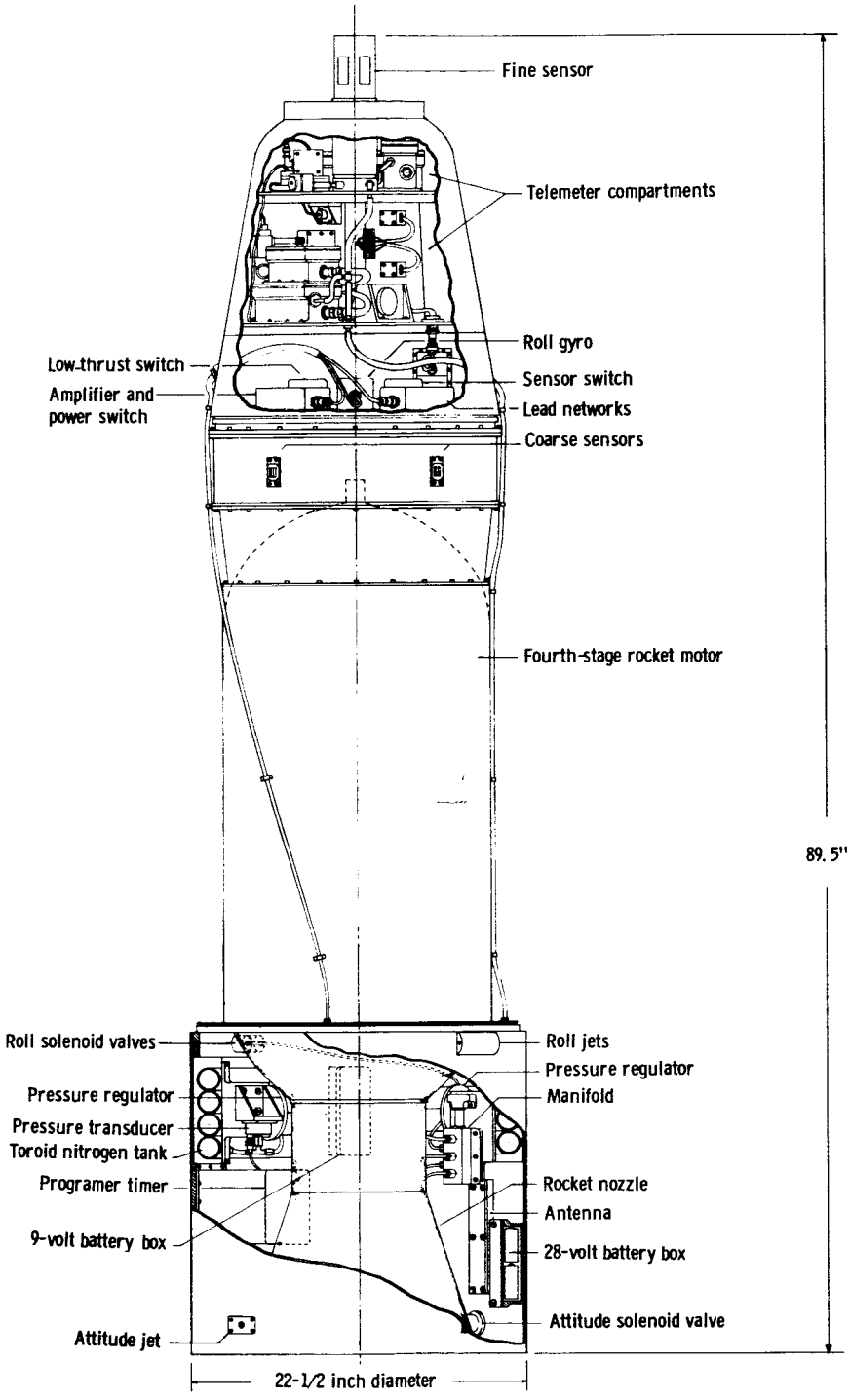

(b) Drawing.

Figure 1.- Concluded.

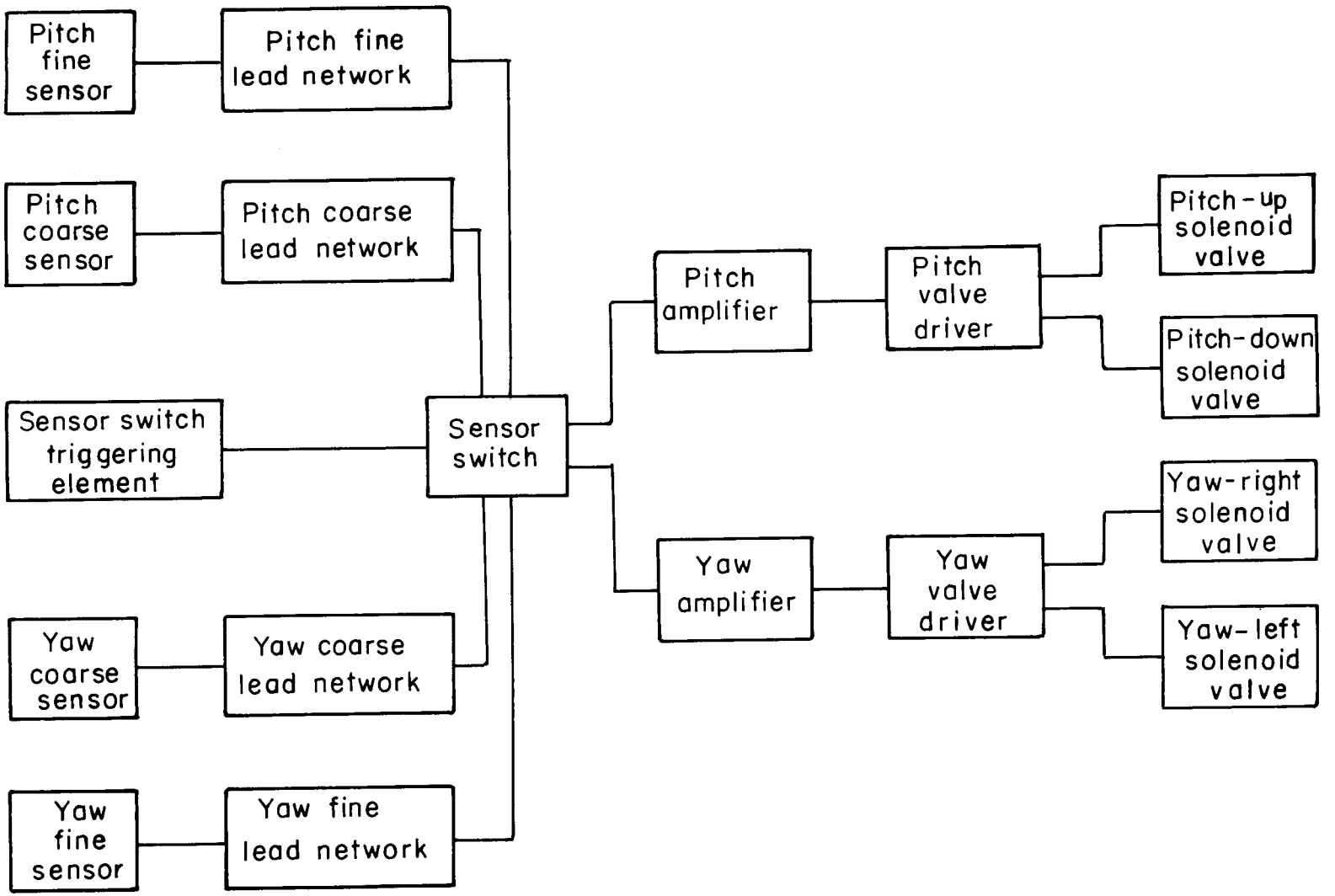

Figure 2.- Block diagram of pitch- and yaw-attitude control system.

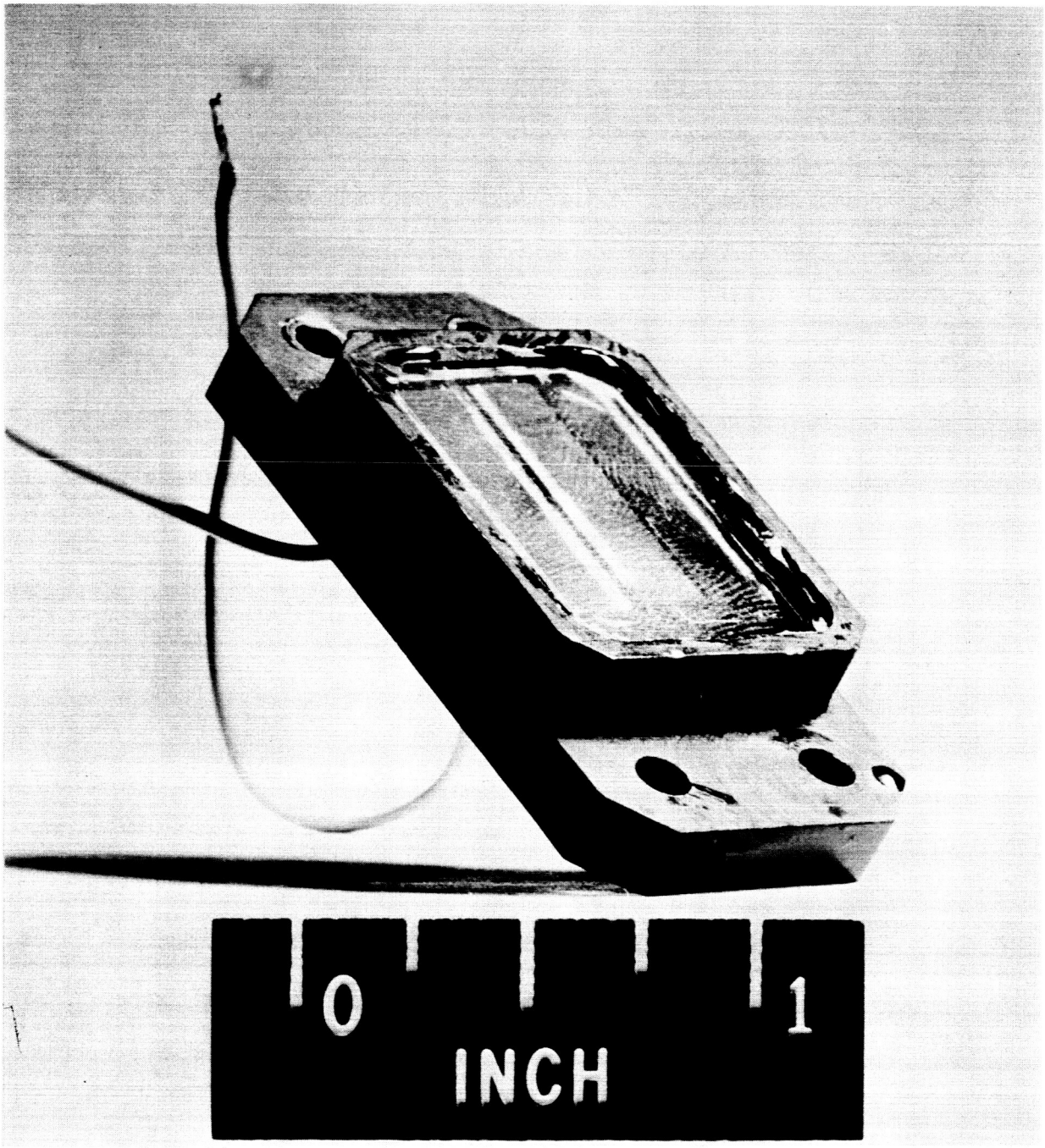

Figure 3.- A single coarse sensing element. L-63-9266

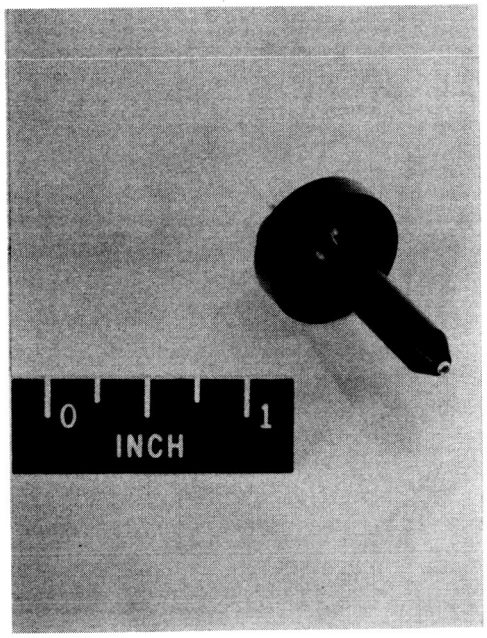

(a) Triggering element assembly.

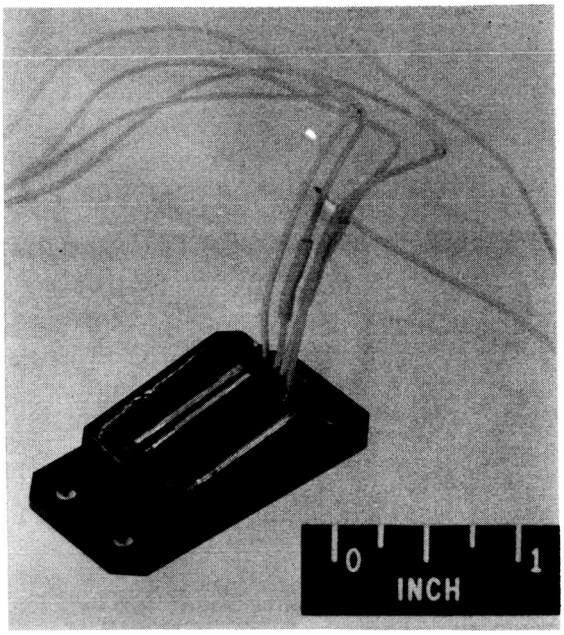

(b) Fine sensing element assembly.

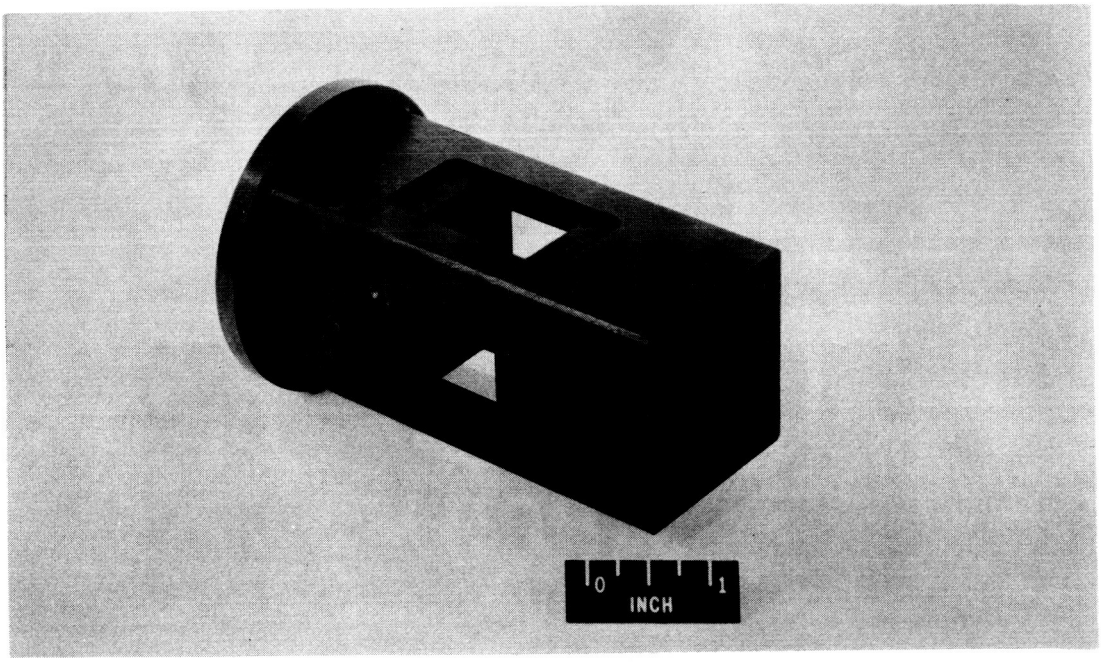

(c) Fine sensor block.

Figure 4.- Fine sensor parts before final assembly. L-63-9267

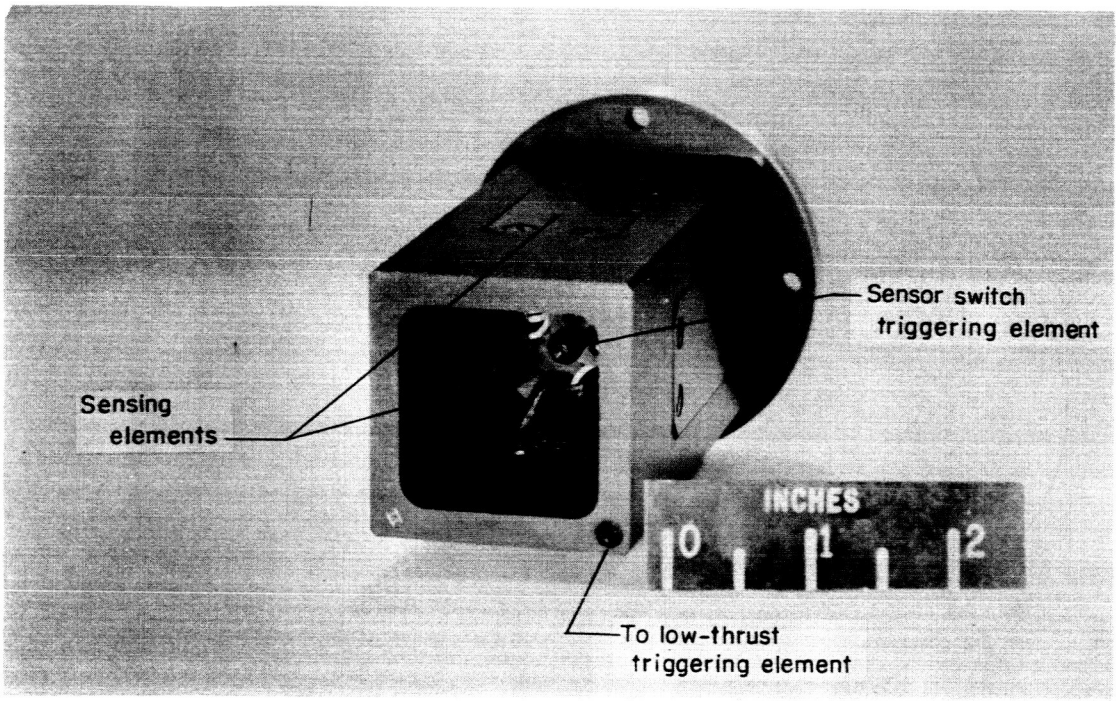

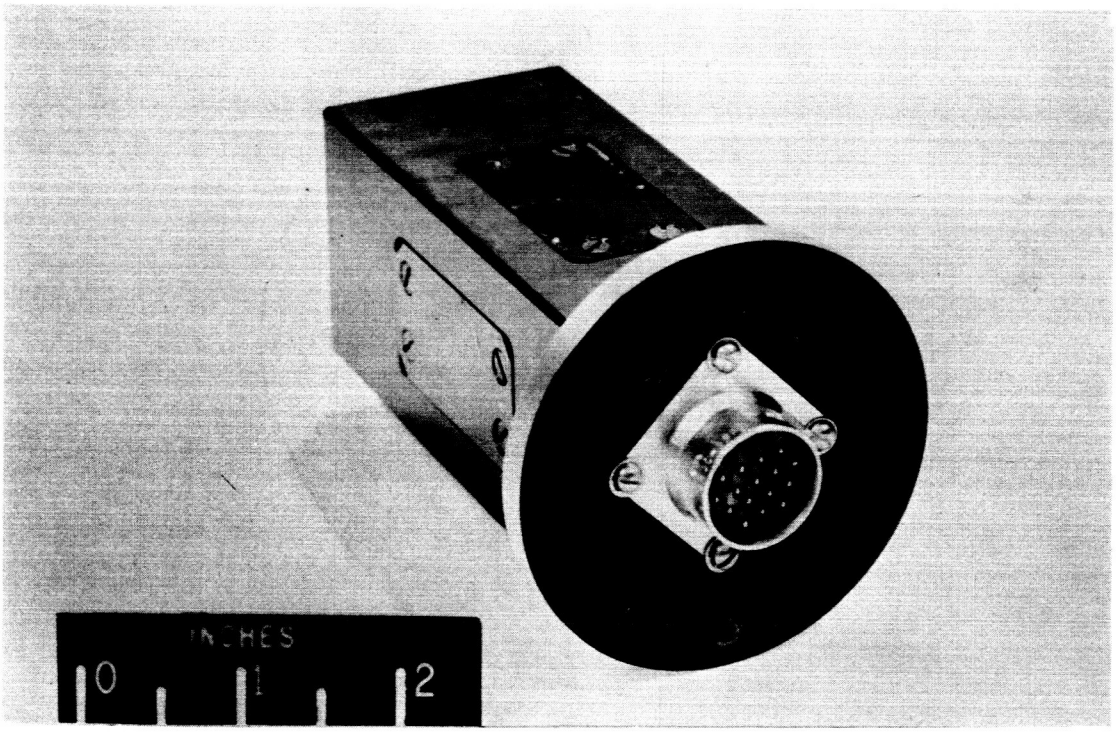

Figure 5.- Two views of the completely assembled fine sensor. L-63-9268

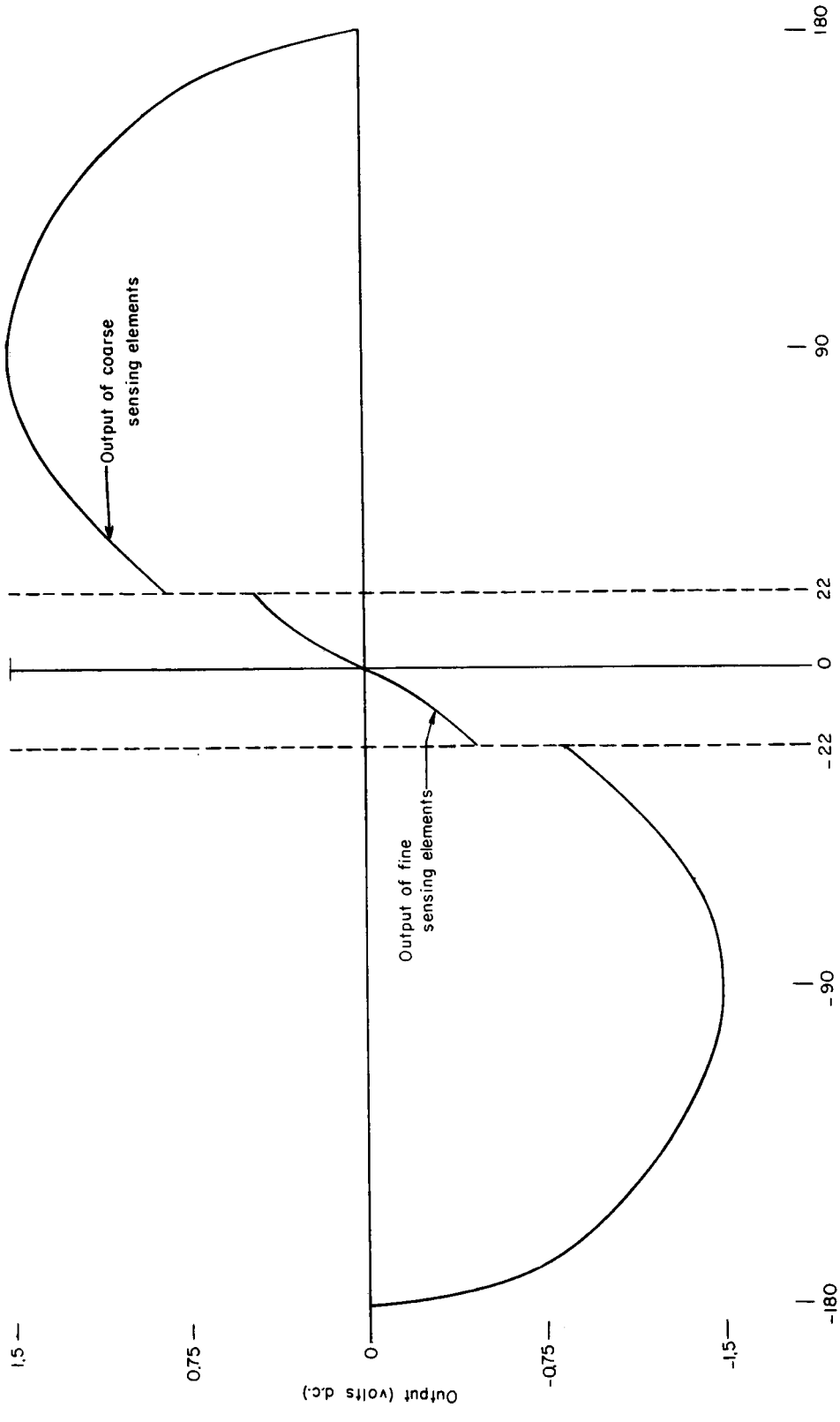

Figure 6.- Single-axis solar sensor output characteristic.

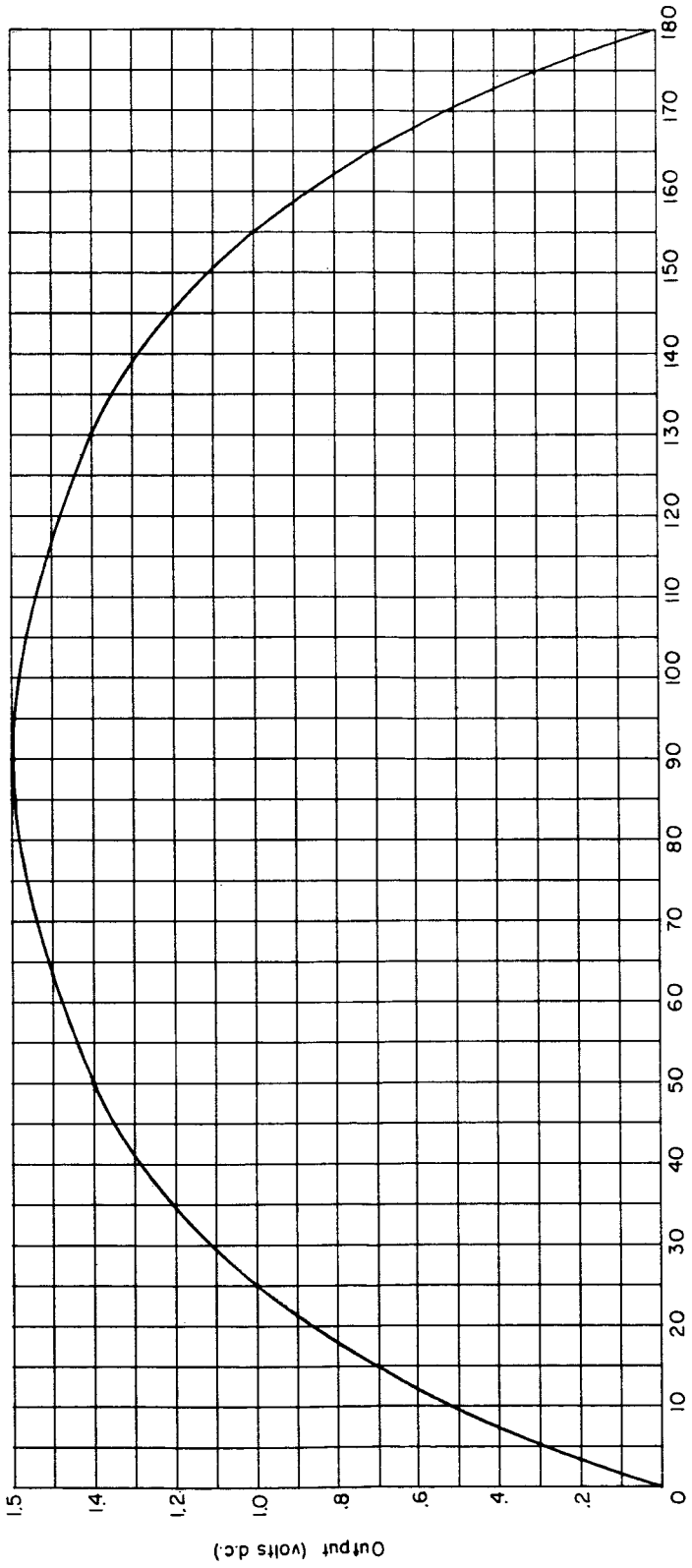

Figure 7.- Coarse sensor output calibration.

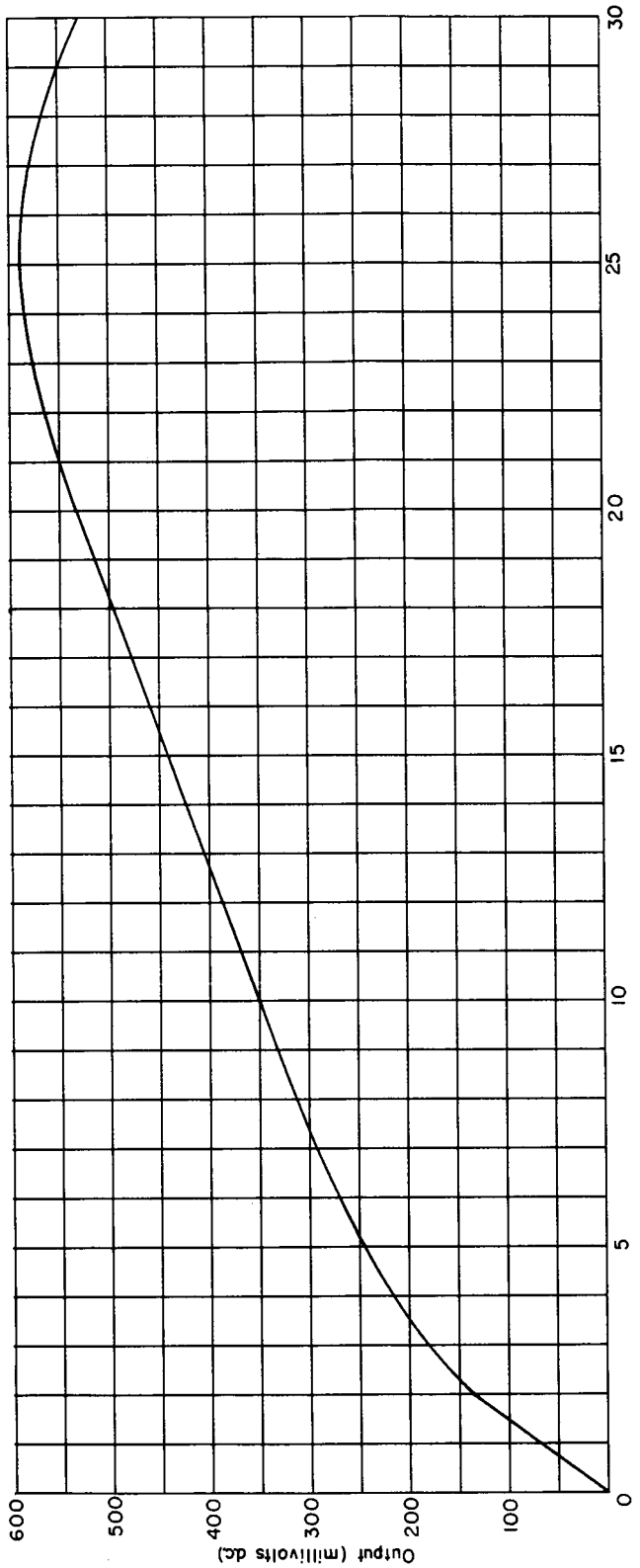

Figure 8.- Fine sensor output calibration.

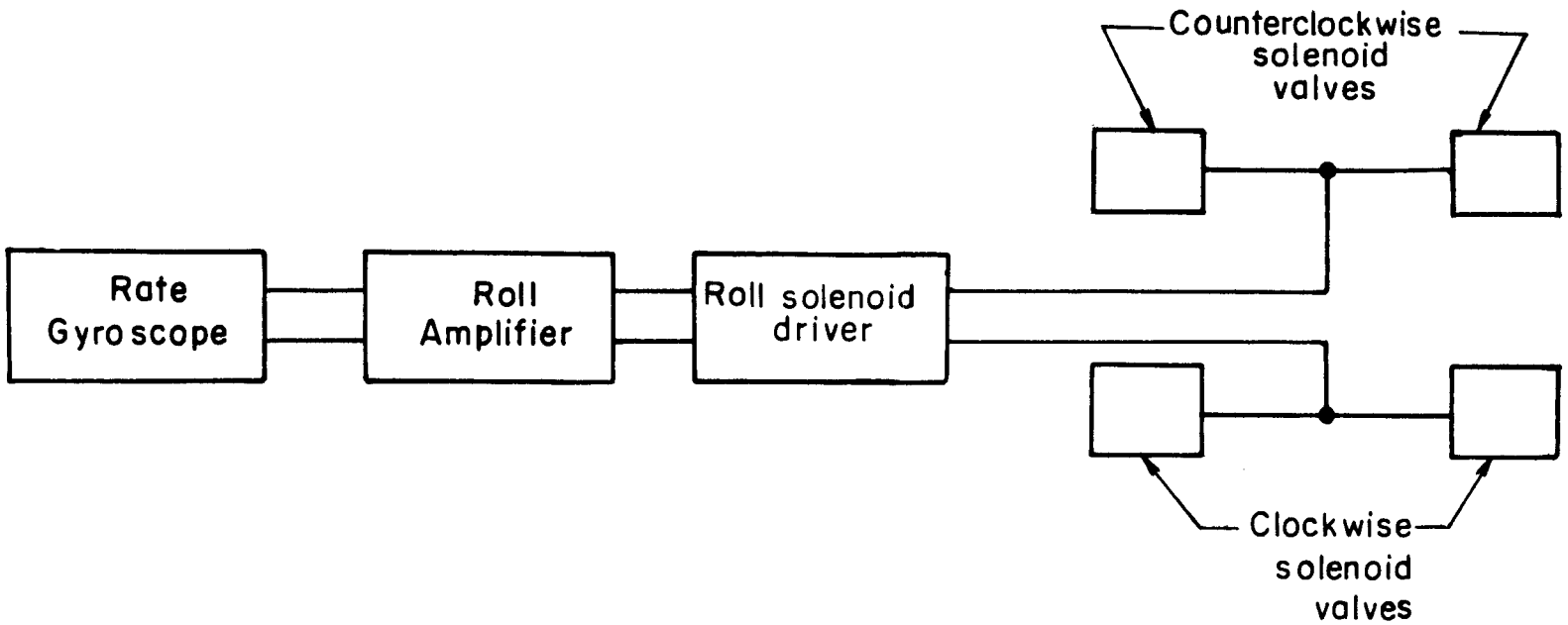

Figure 9.- Block diagram of roll-rate control system.

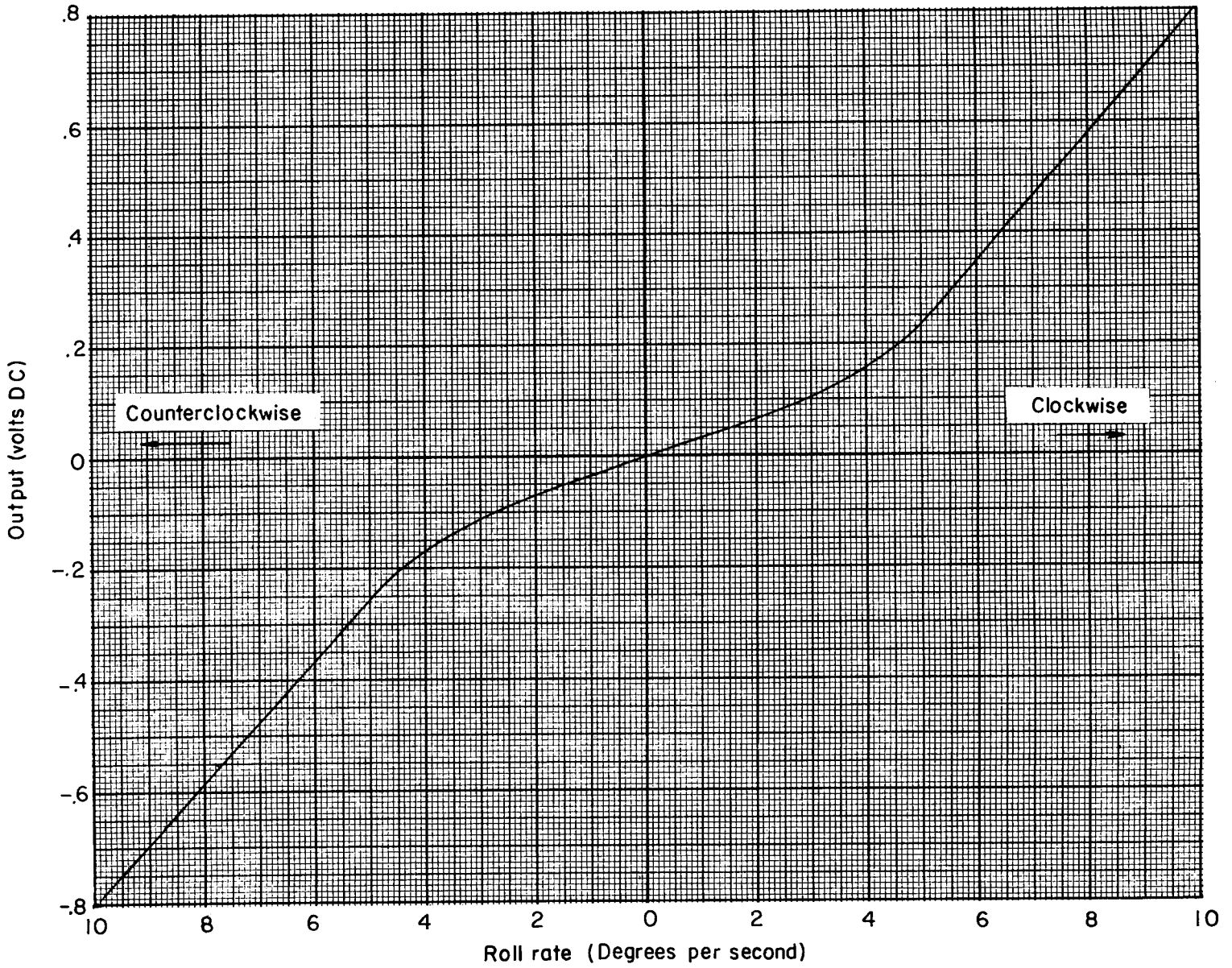

Figure 10.- Rate gyroscope output calibration.

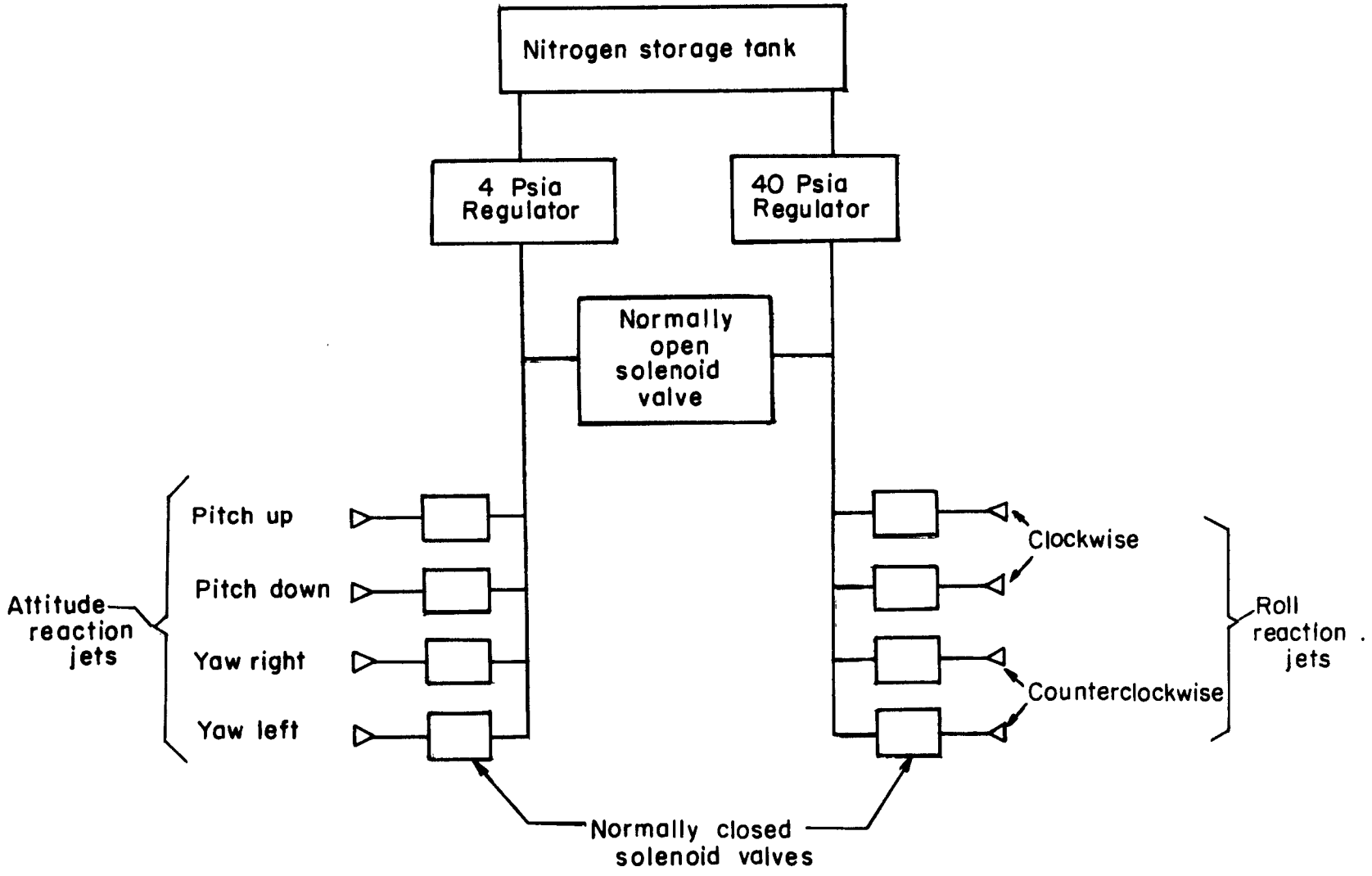

Figure 11.- Schematic diagram of pneumatic system.

(a) Nitrogen storage tank. L-62-2896

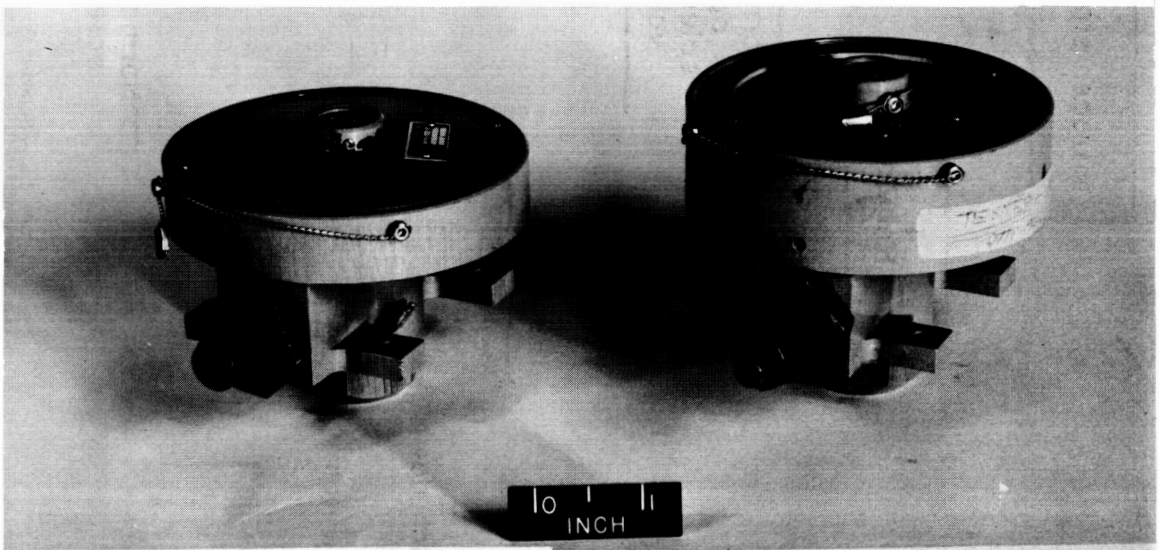

40 lbs/sq in. Regulator
Operating inlet pressure : 200 to 3100 lbs/sq in.
Flow rate: Minimum of 0.40 pounds of gaseous nitrogen per minute at 40 lbs/sq in.

4 lbs/sq in. Regulator
Operating inlet pressure : 200 to 3100 lbs/sq in.
Flow rate; Minimum of 0.02 pounds of gaseous nitrogen per minute at 4 lbs/sq in.
Designed to withstand 40 lbs/sq in. back pressure

(b) Pressure regulators.

Figure 12.- Components of the pneumatic system. L-63-9409

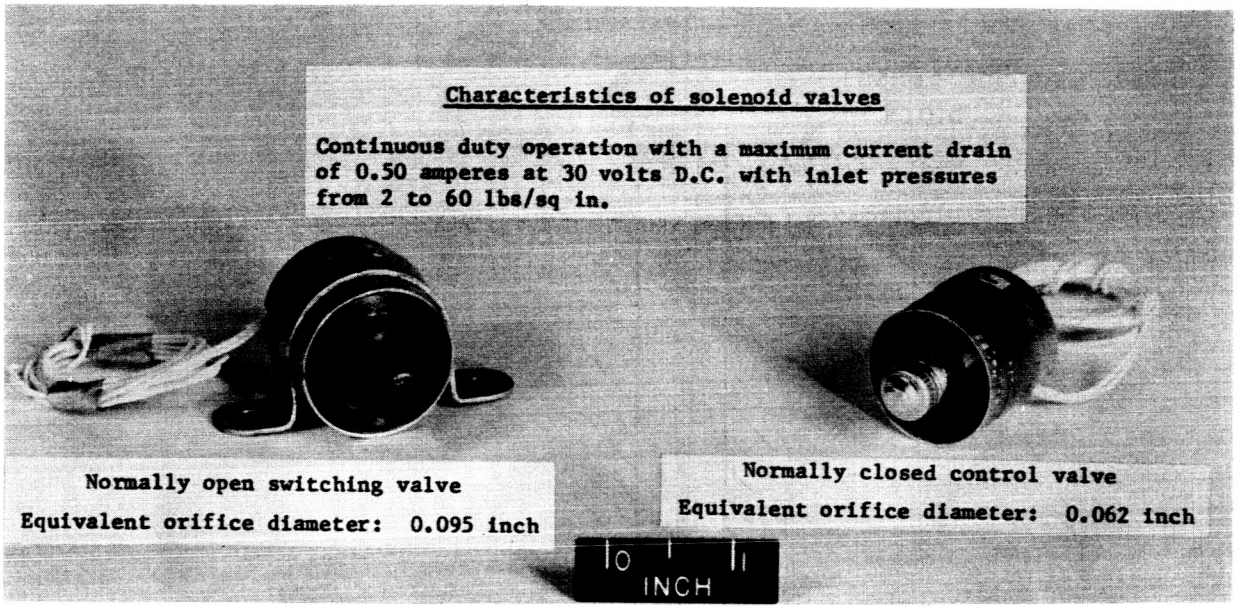

(c) Solenoid valves.

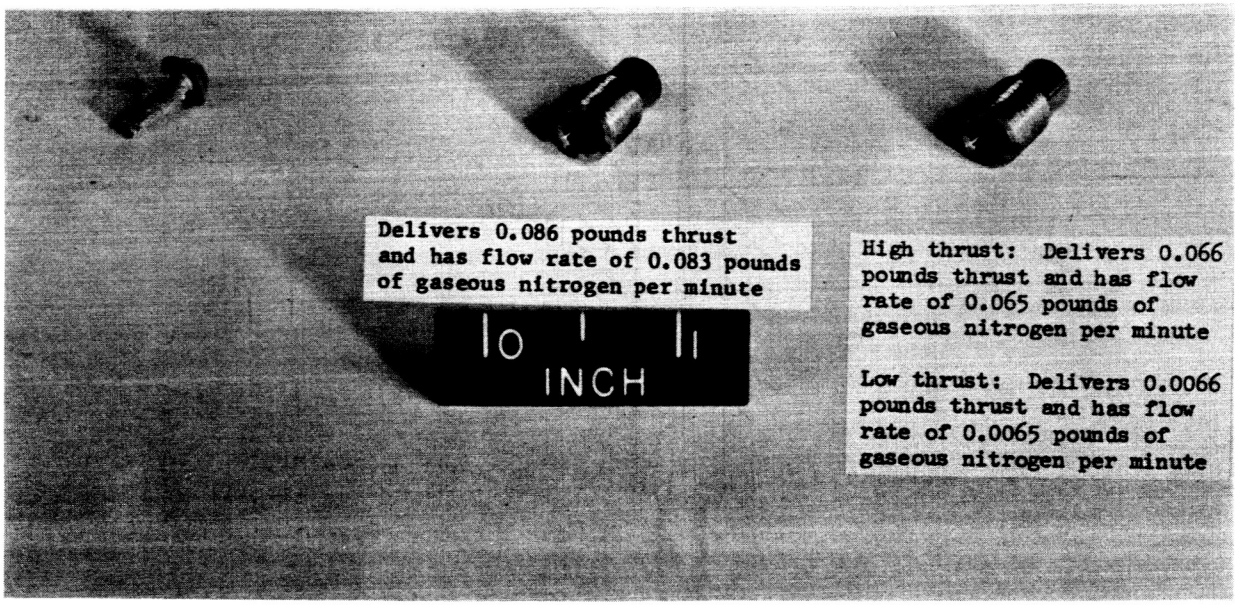

(d) Filter (25 micron). (e) Roll-control nozzle. (f) Attitude-control nozzle.

Figure 12.- Concluded. L-63-9269

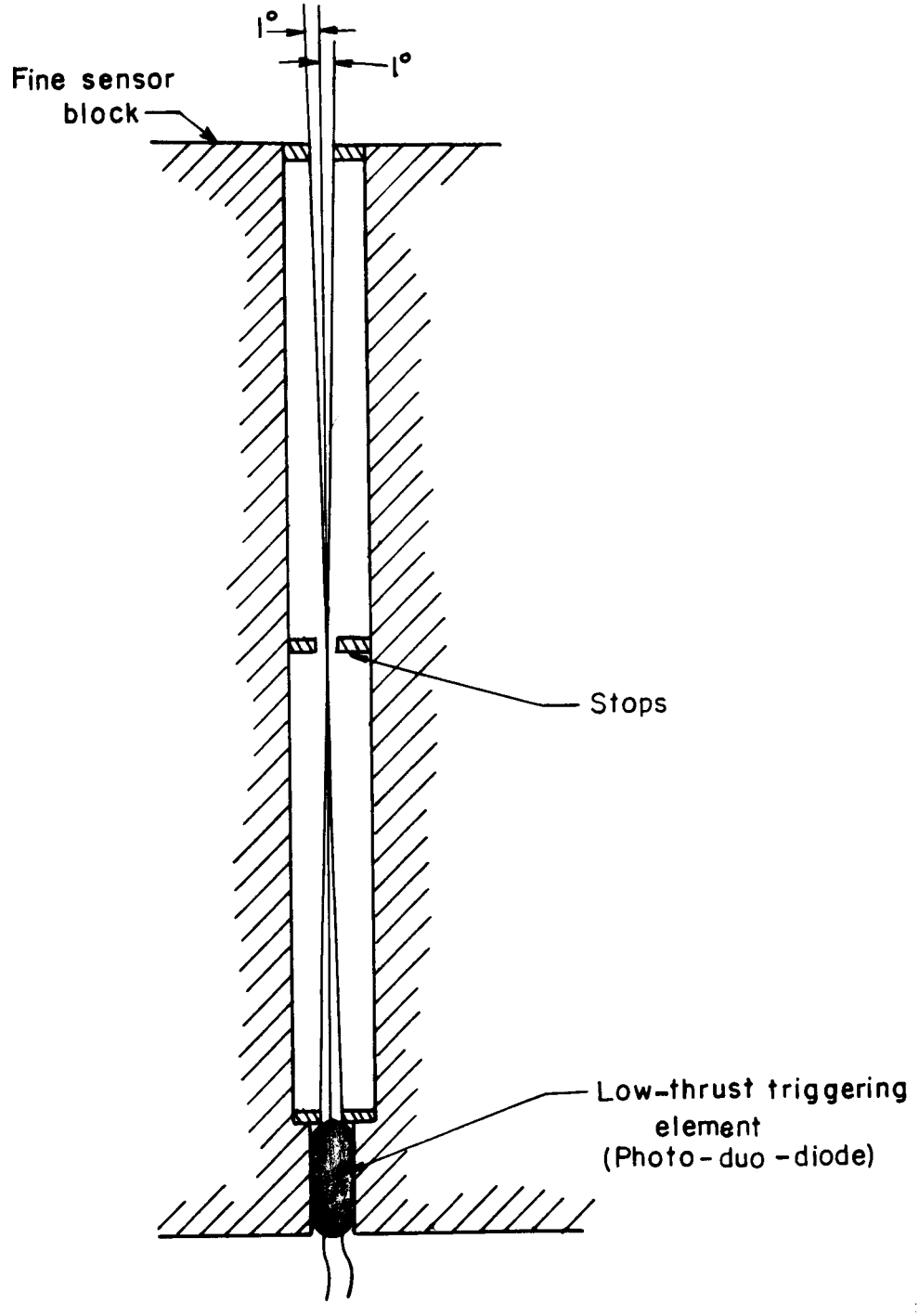

Figure 13.- Mounting of low-thrust triggering element in fine sensor block.

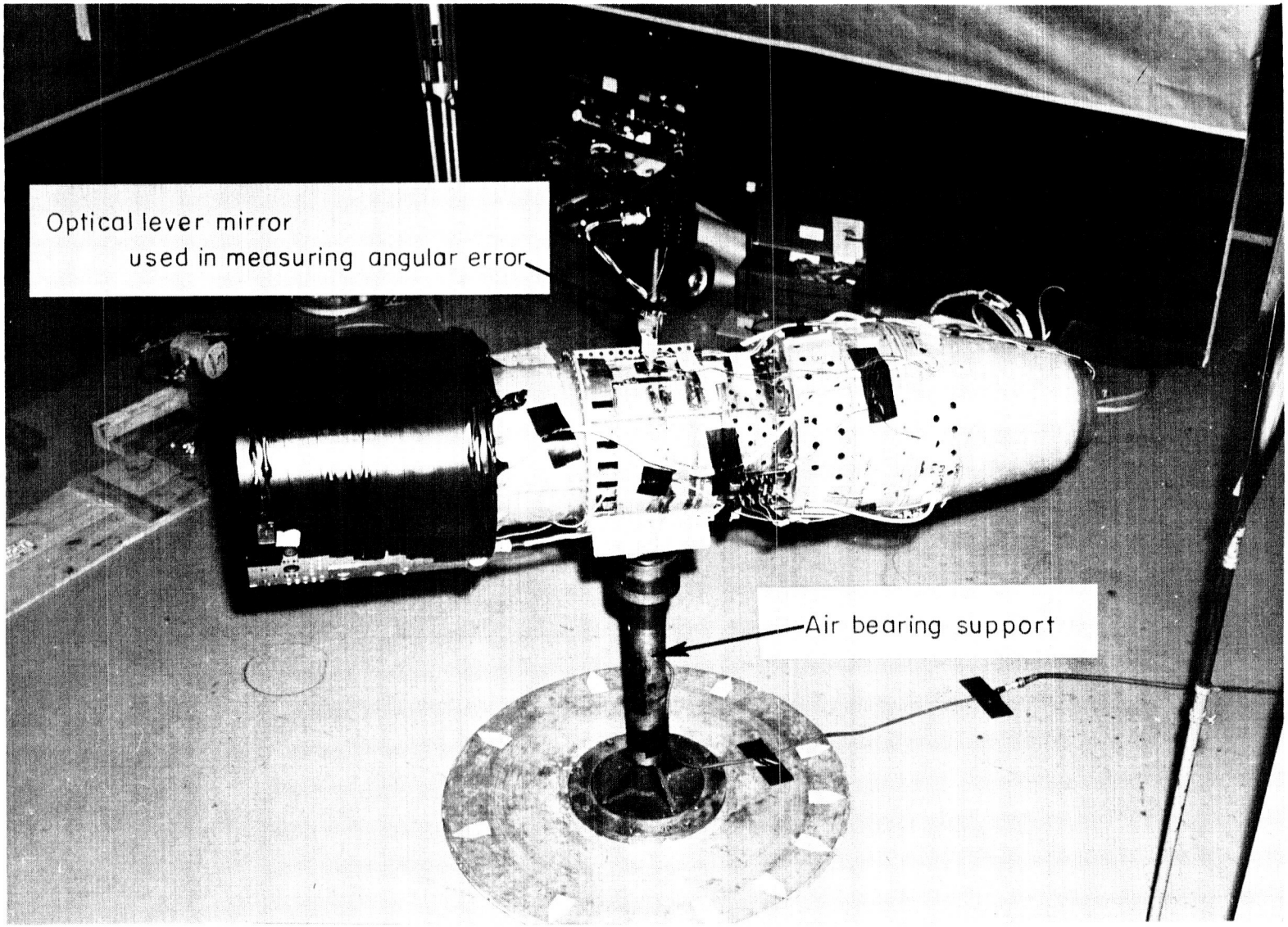

Figure 14.- Pitch- and yaw-attitude control-system test configuration. L-63-4677

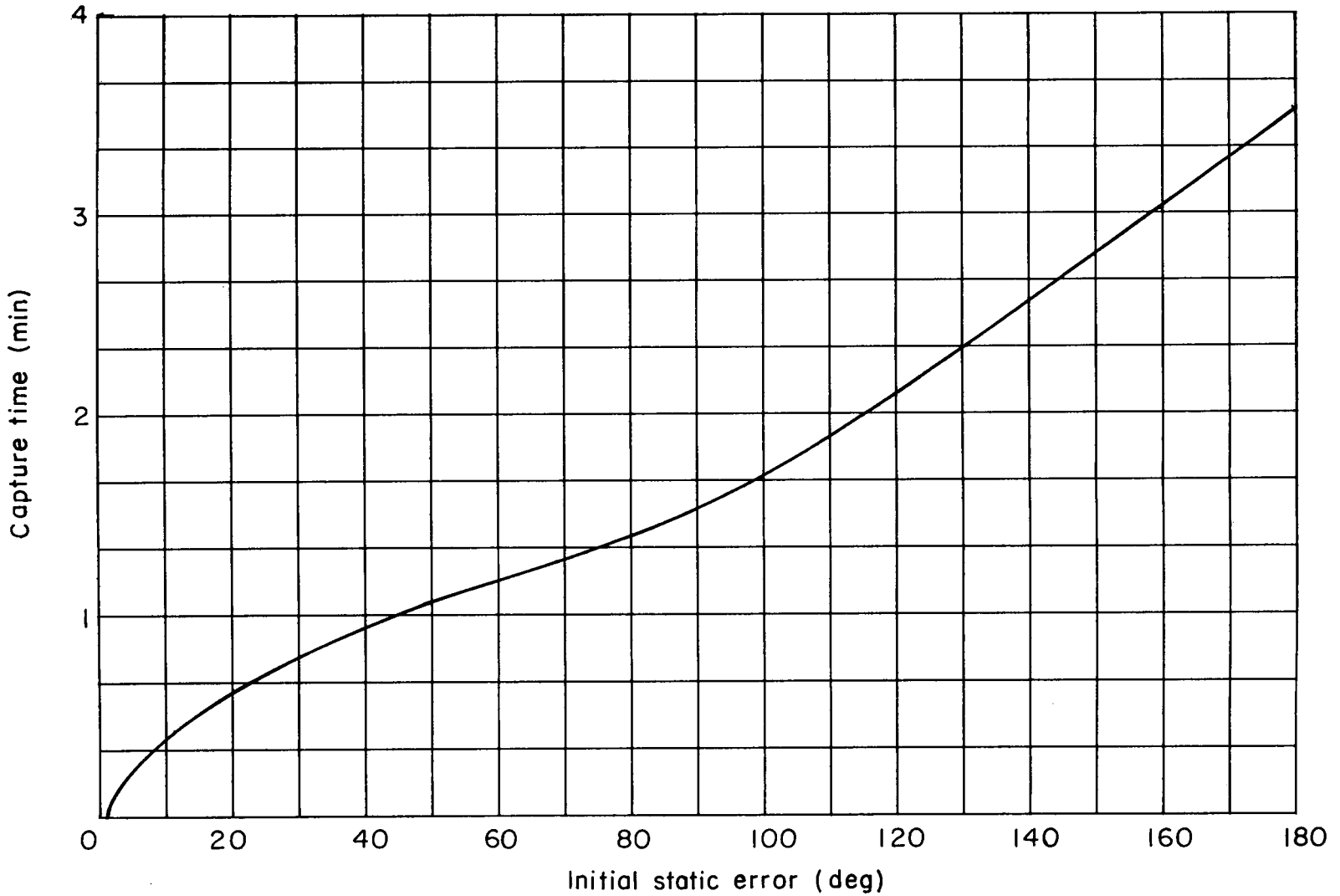

Figure 15.- Laboratory capture test results.

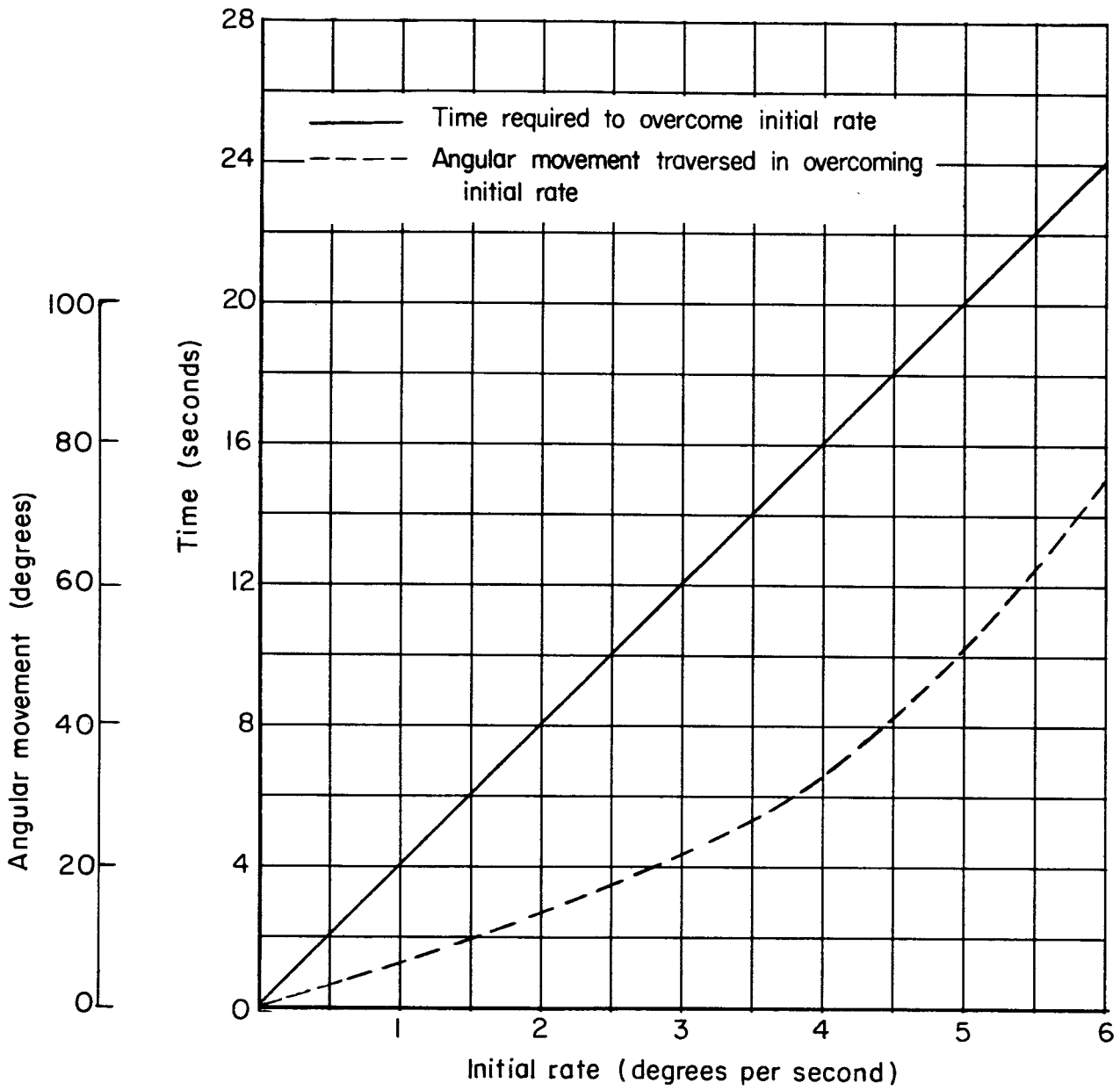

Figure 16.- Laboratory initial angular rate test results.

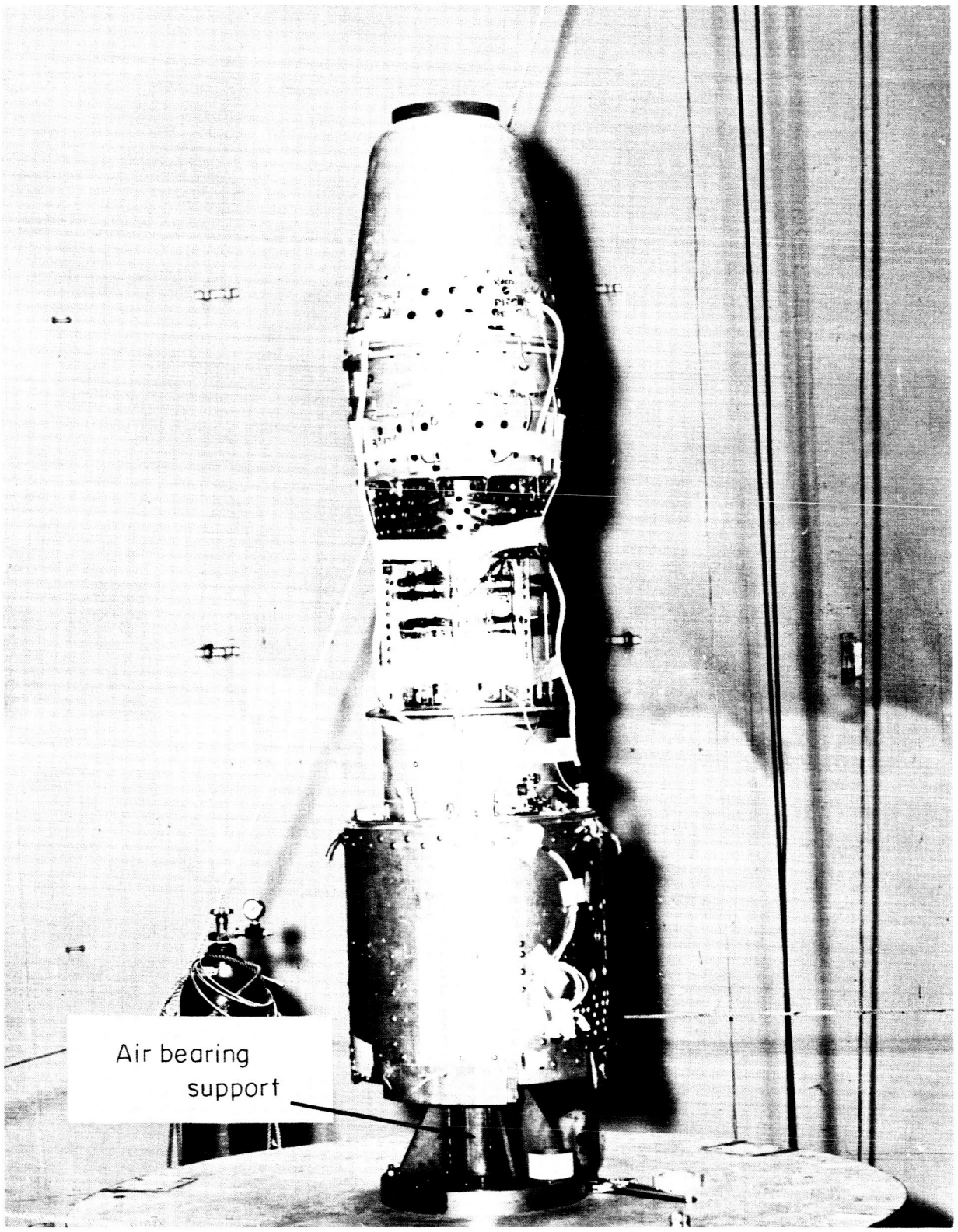

Figure 17.- Roll-rate control-system test configuration. L-63-4155.1

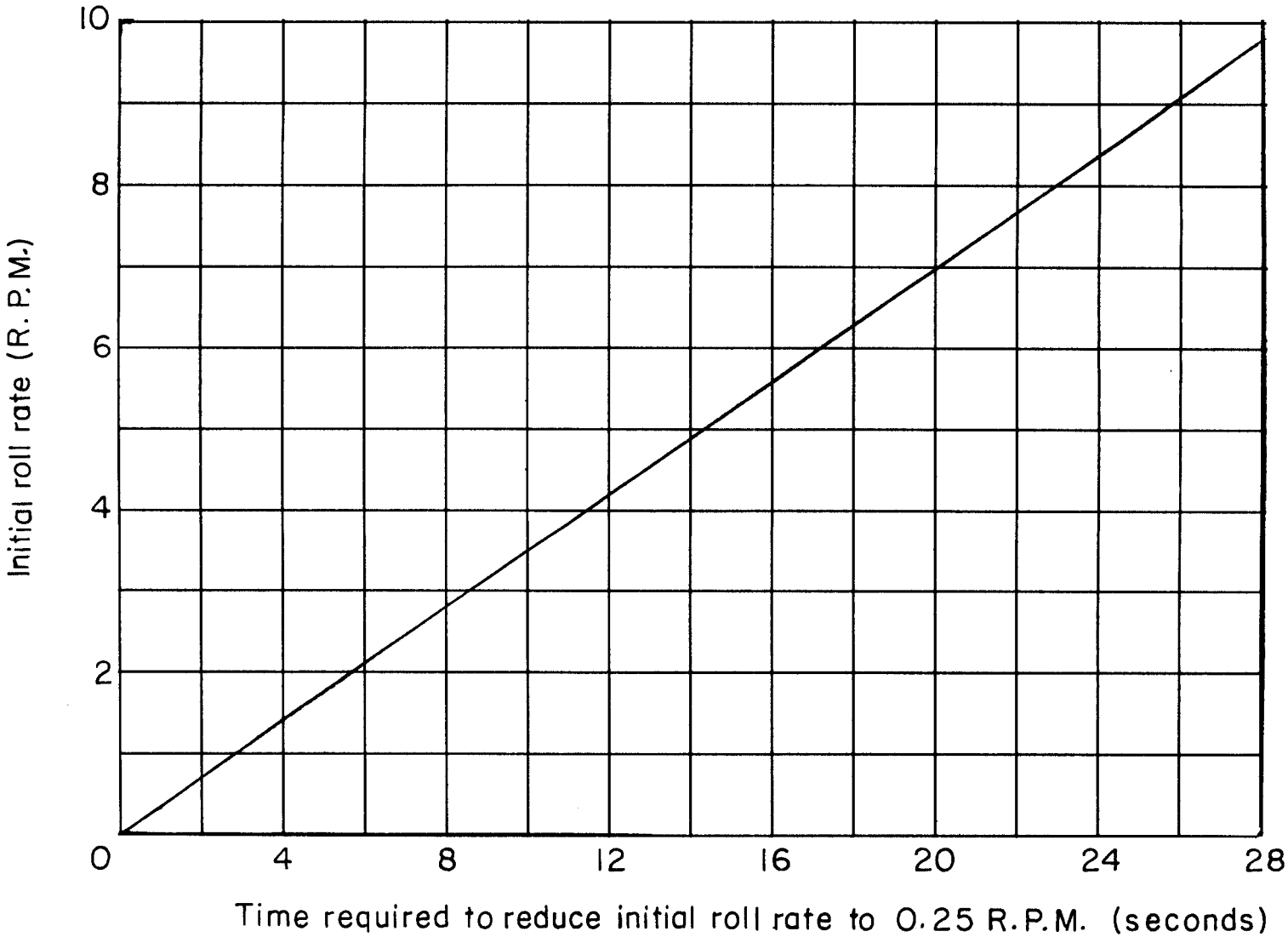

Figure 18.- Laboratory roll-rate test results.

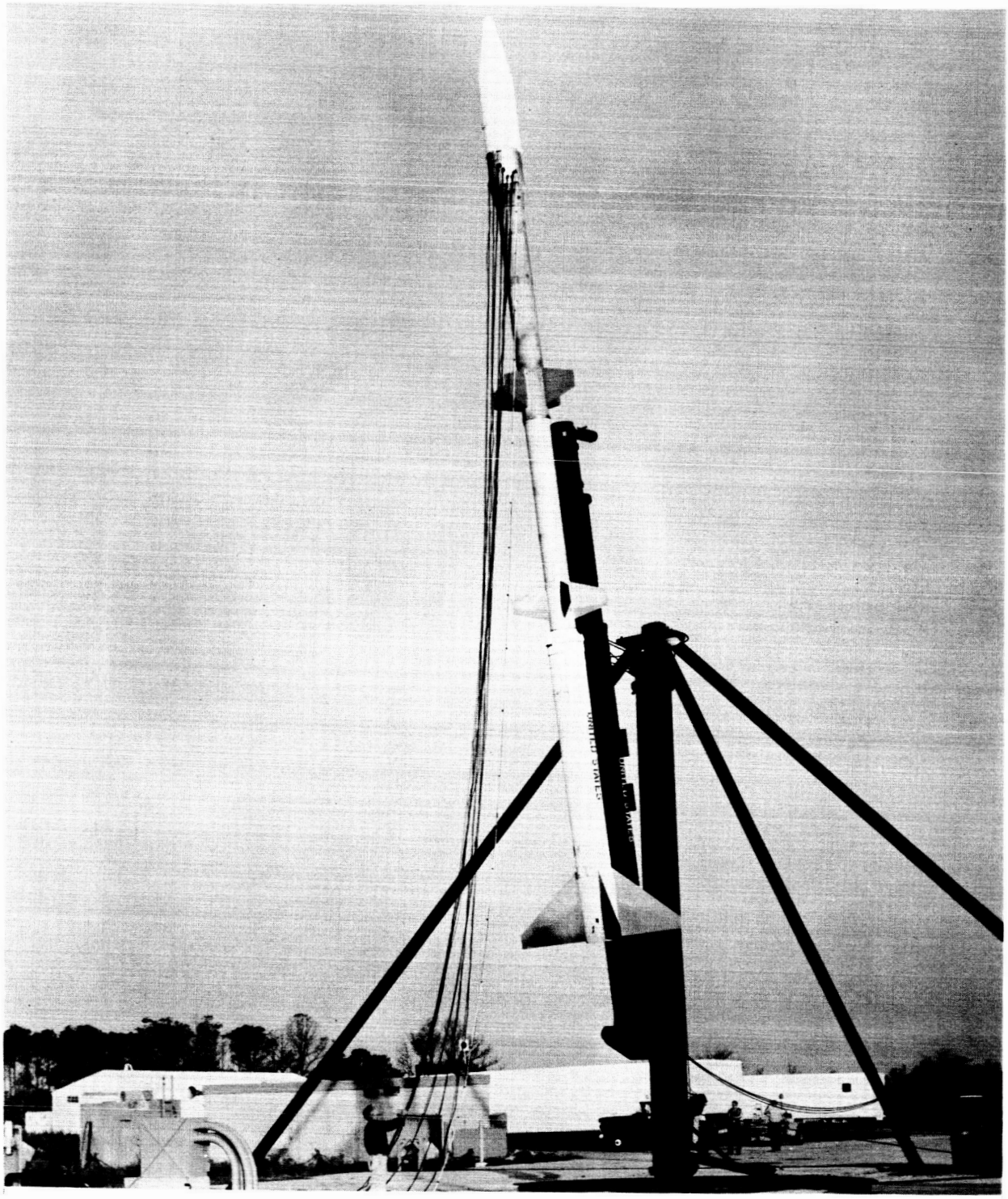

Figure 19.- Vehicle and spacecraft on launcher. L-63-7978

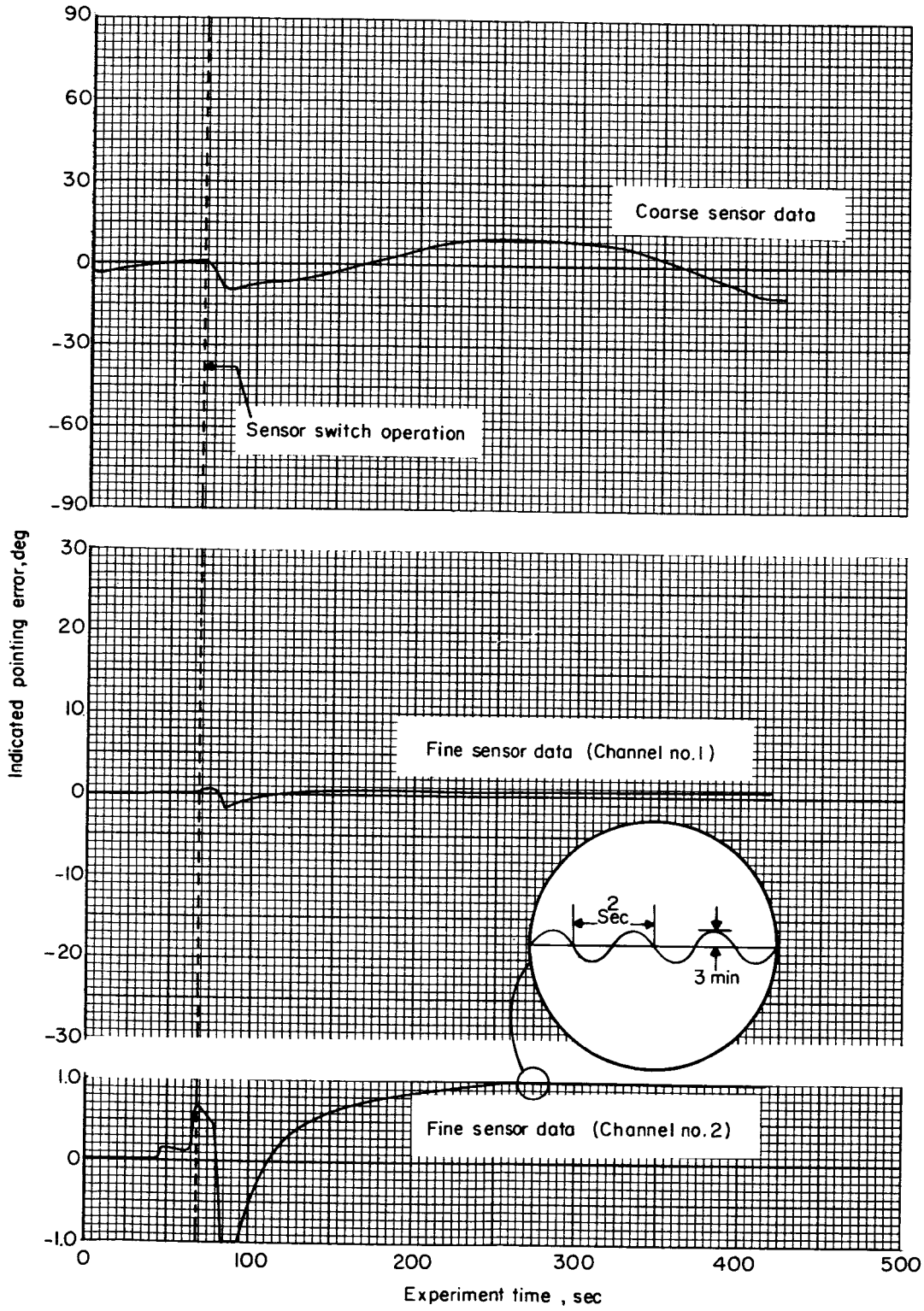

Figure 20.- Pitch-axis telemetry data.

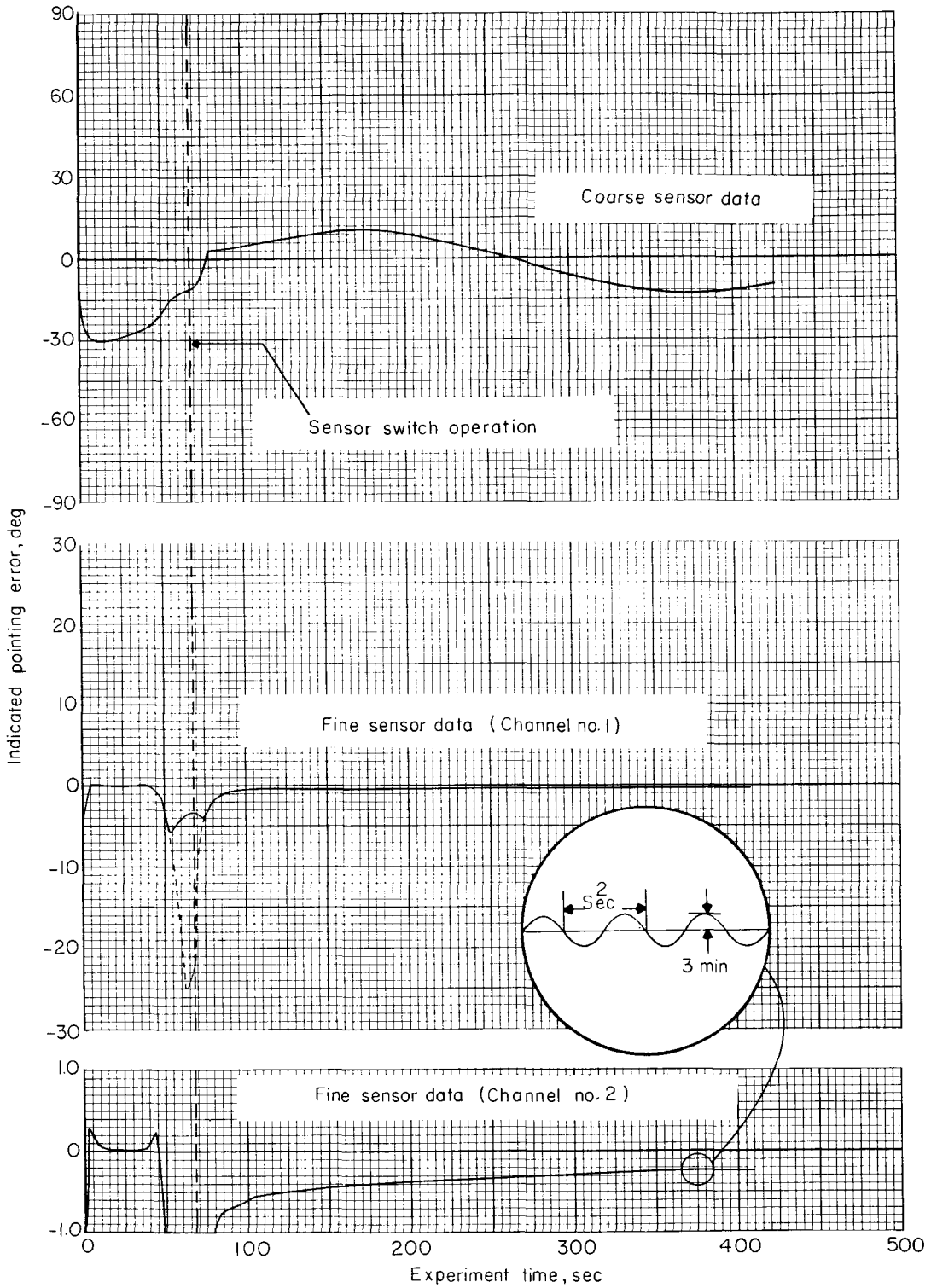

Figure 21.- Yaw-axis telemetry data.

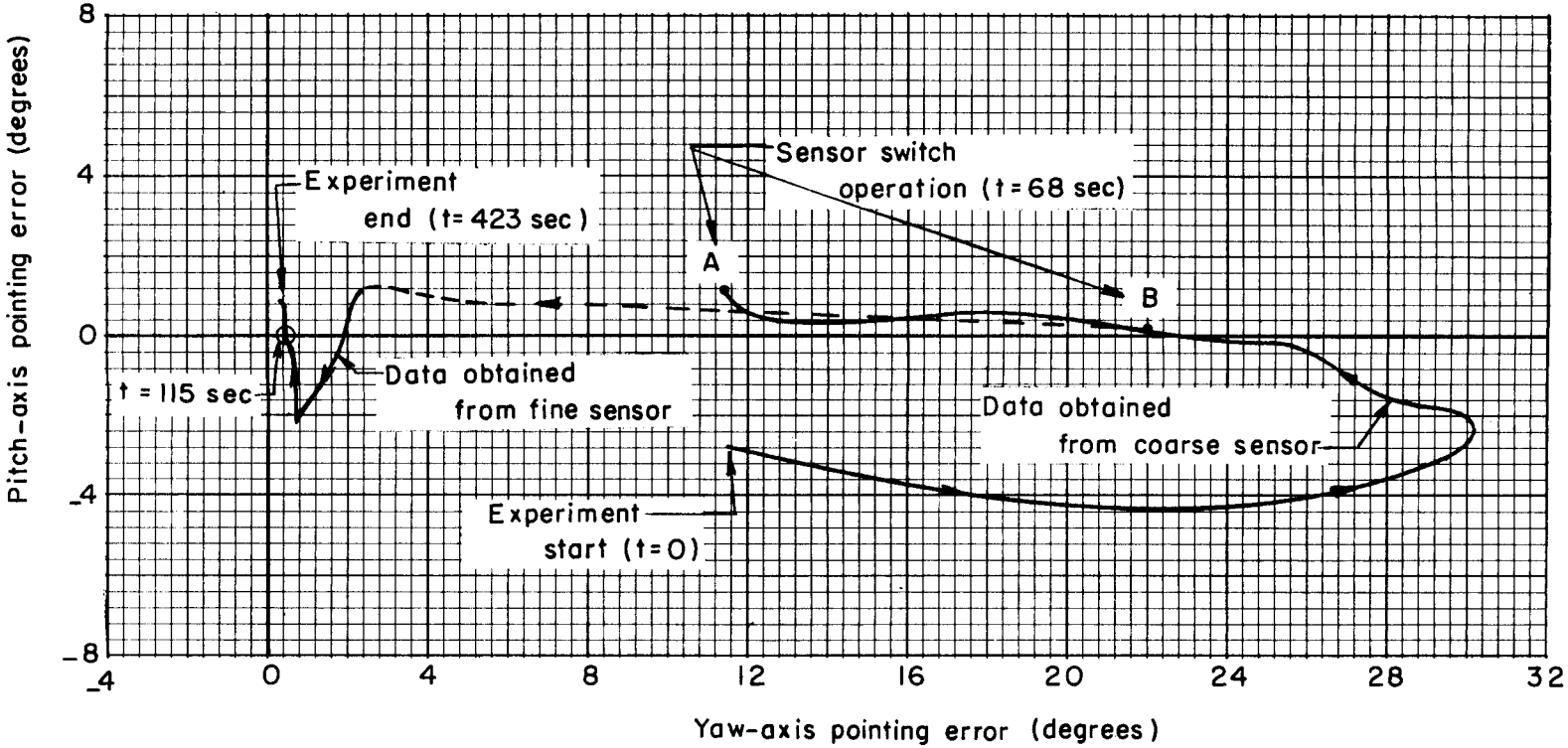

Figure 22.- Two-axis pointing error.

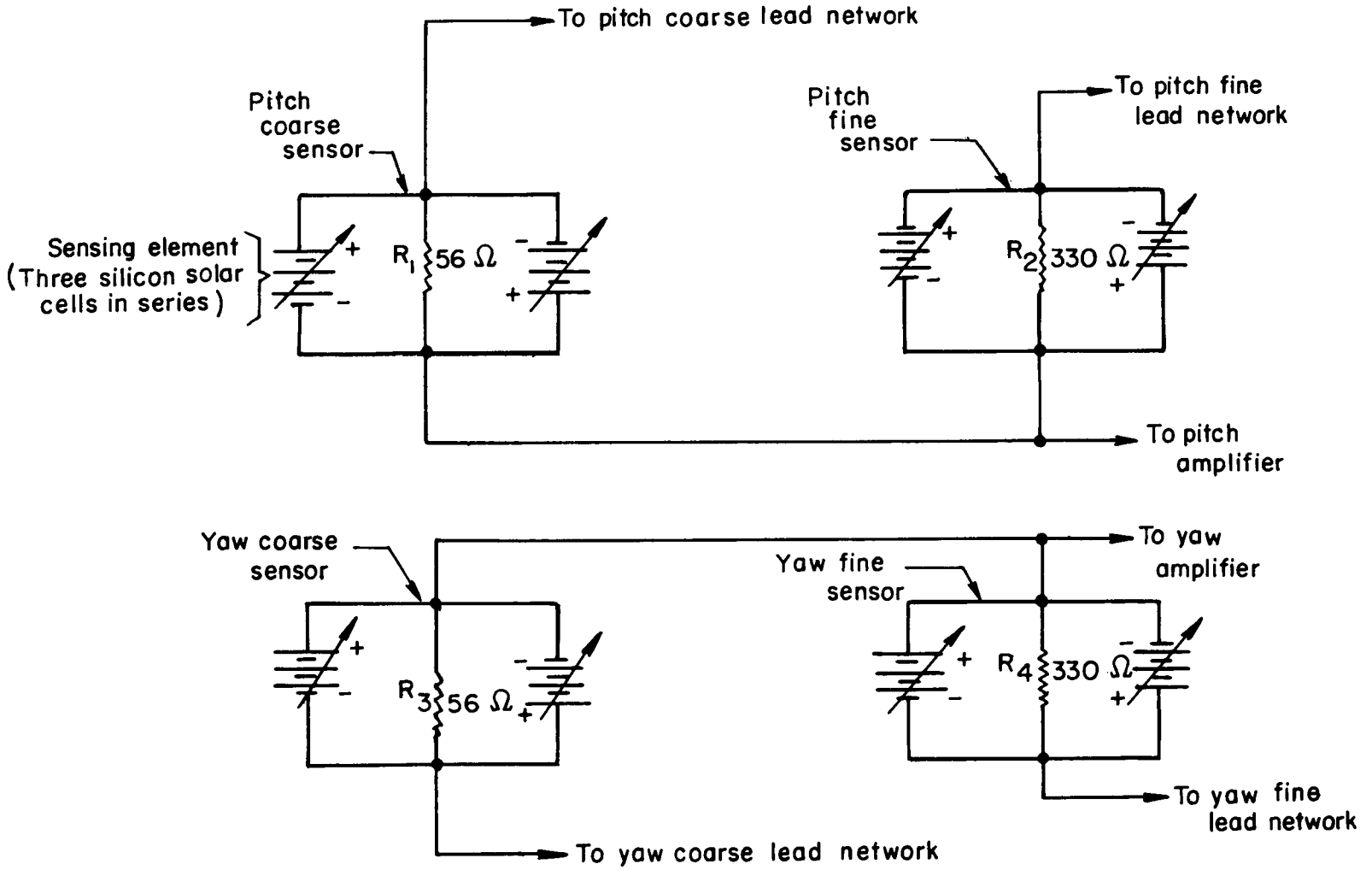

Figure 23.- Solar sensor schematic diagram.

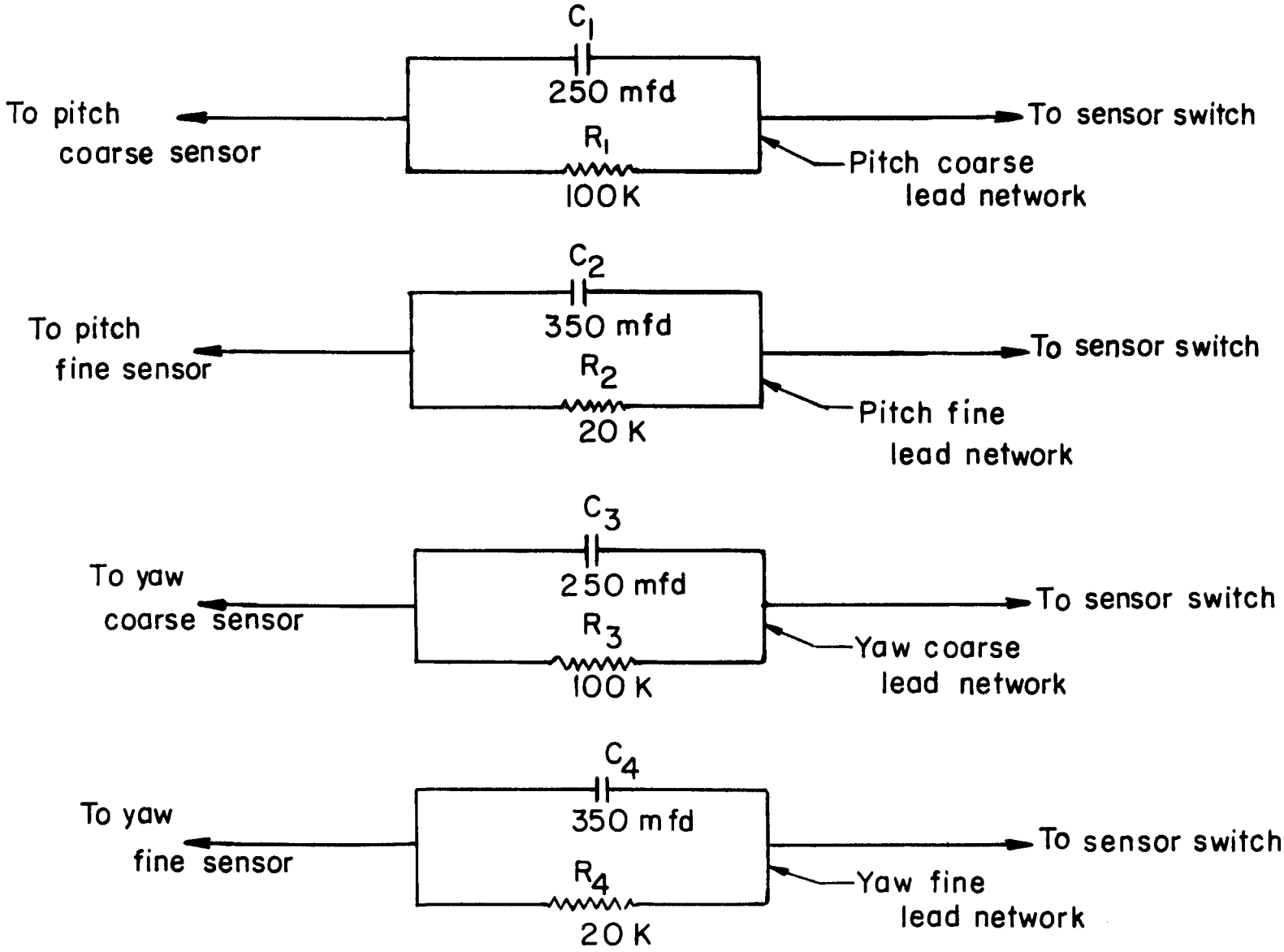

Figure 24.- Schematic diagram of lead networks.

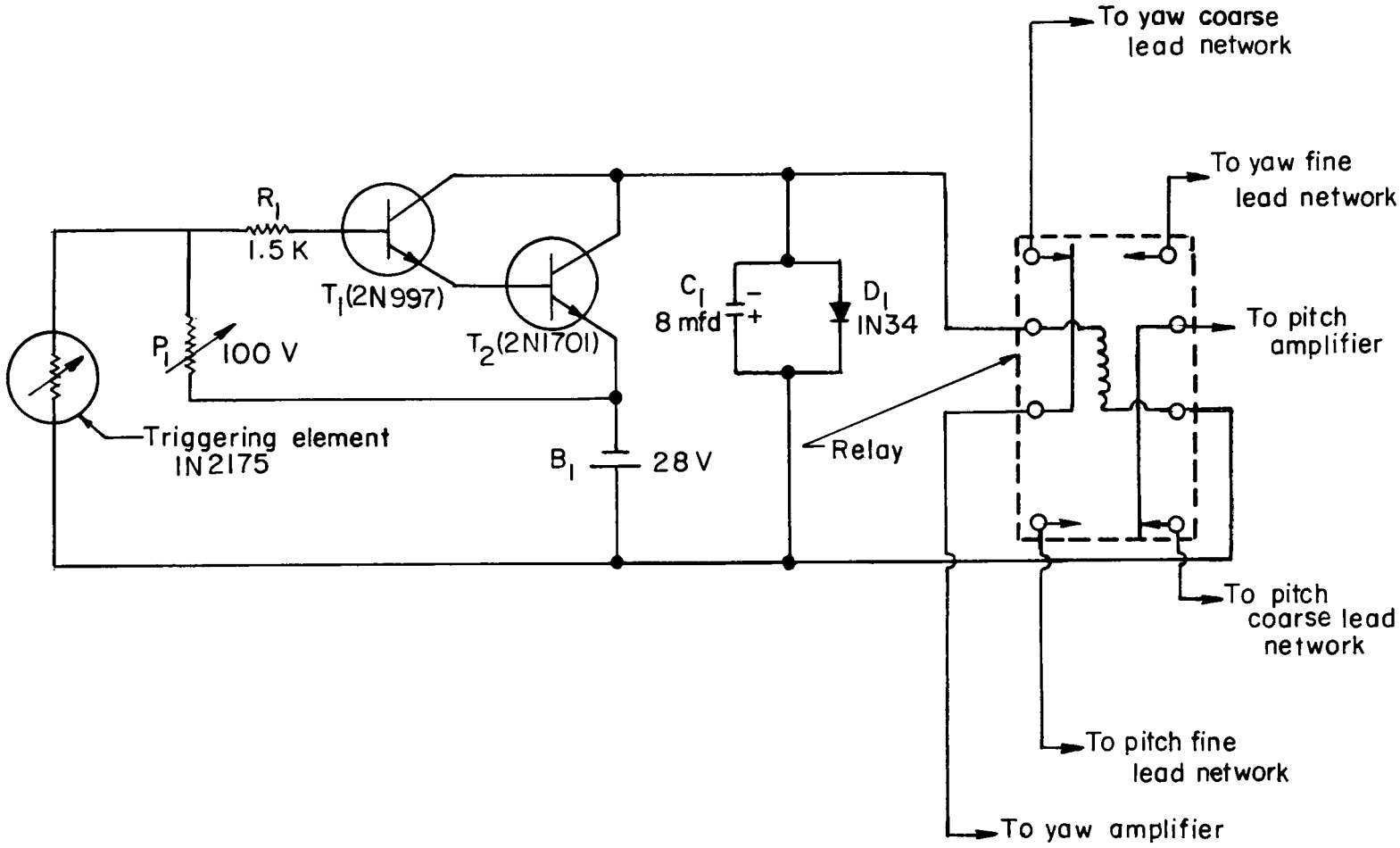

Figure 25.- Schematic diagram of sensor switch.

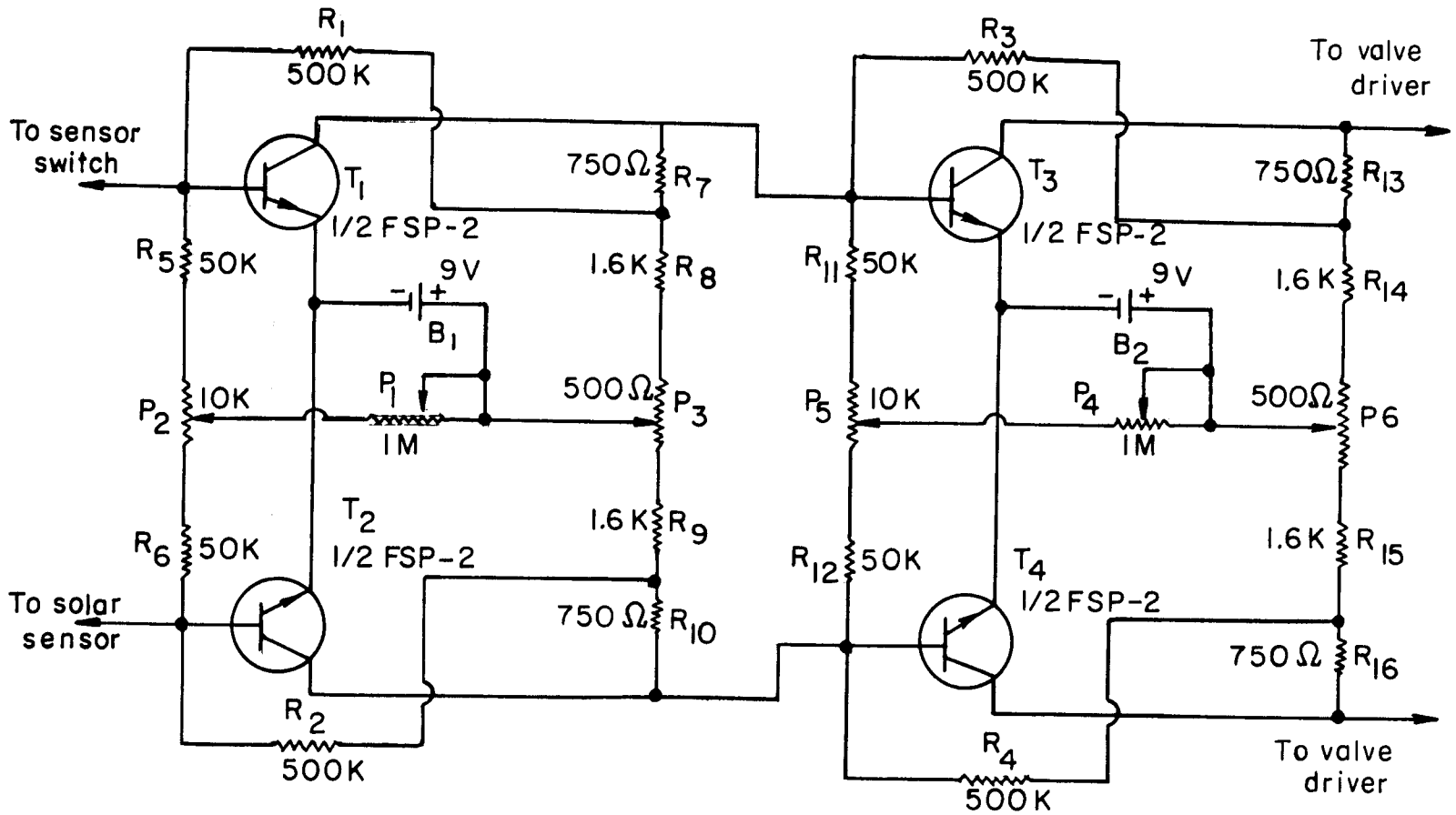

Figure 26.- Pitch amplifier schematic diagram (yaw amplifier identical).

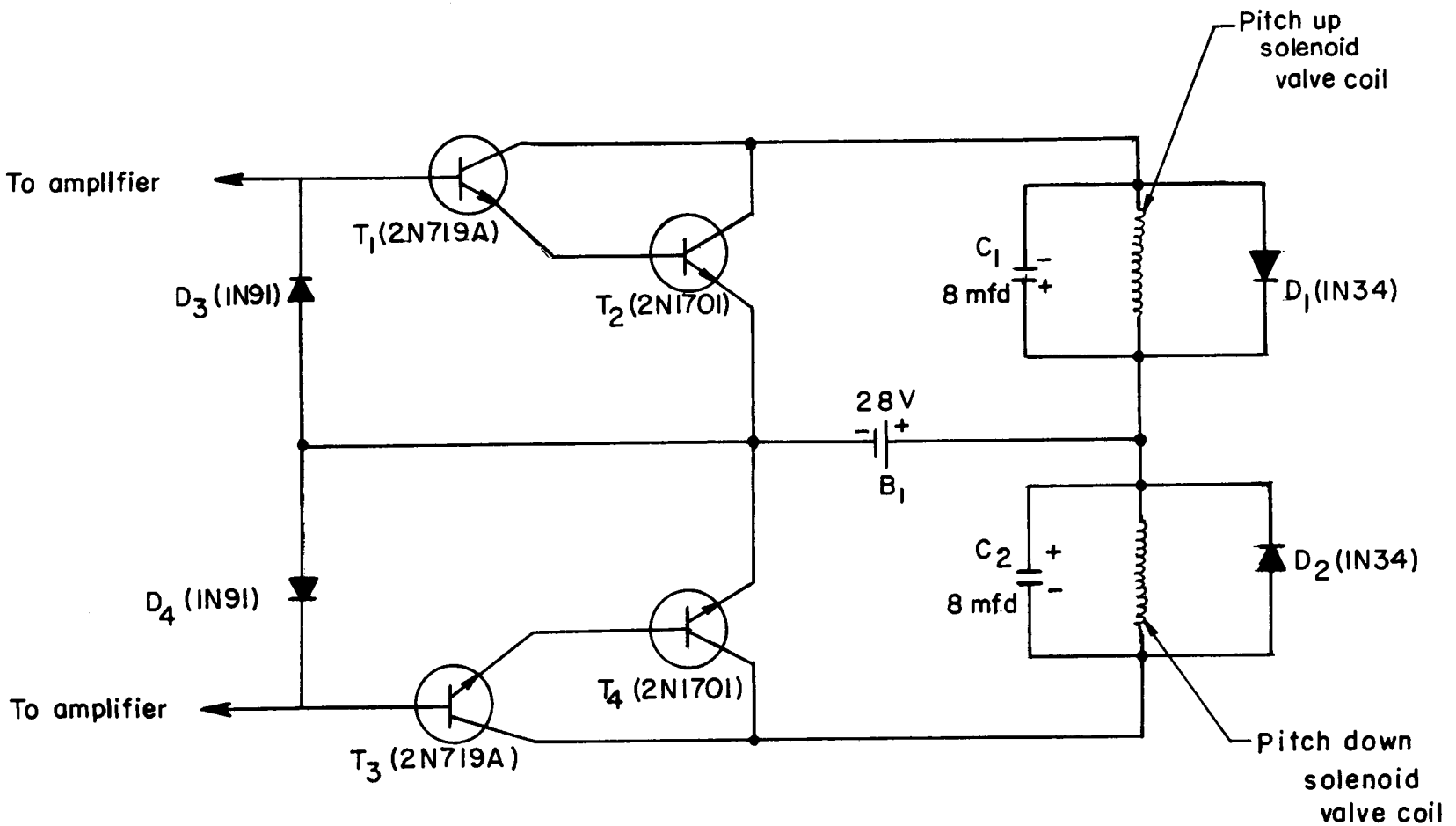

Figure 27.- Pitch valve driver schematic diagram (yaw valve driver identical).

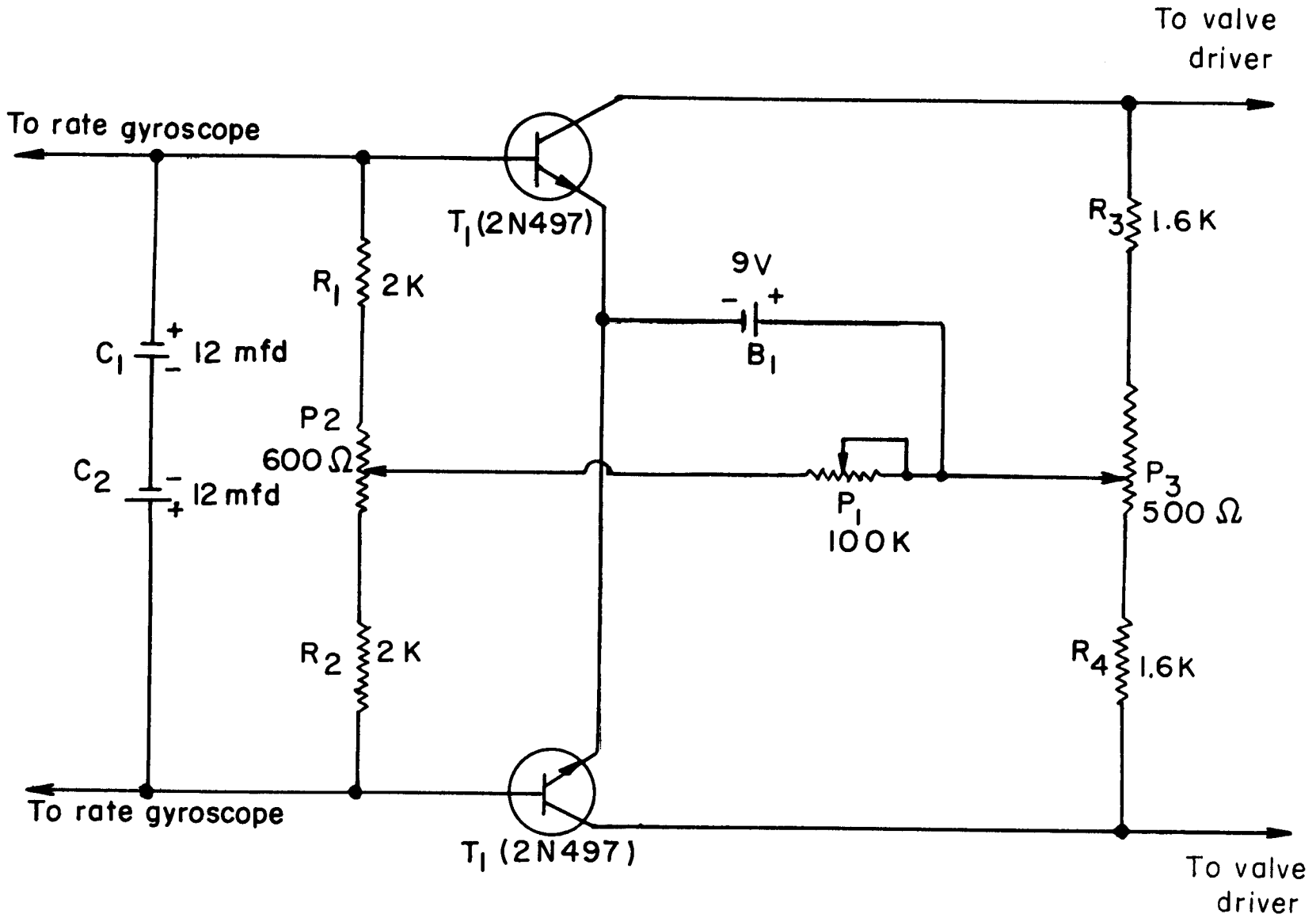

Figure 28.- Roll amplifier schematic diagram.

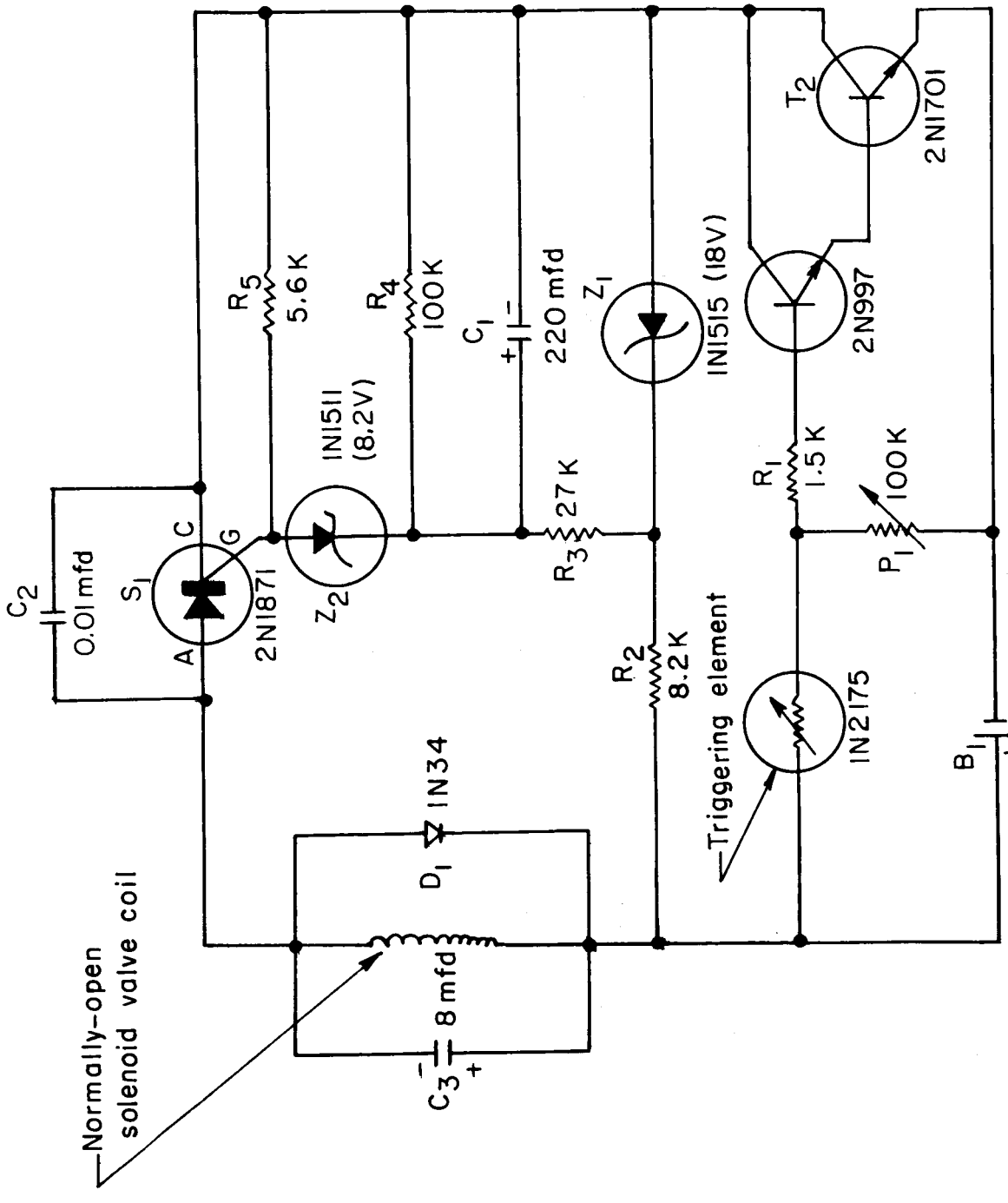

Figure 29.- Low-thrust switch schematic diagram.

NASA-Langley, 1964 L-3925